AGU100 ADVANCING EARTH AND SPACE SCIENCE

Water Resources Research

RESEARCH ARTICLE
10.1029/2018WR022743

Key Points:
- A new synthetic streamflow rescaling method for scenario discovery is introduced
- The method discovers flood risks caused by multiple mechanisms beyond mean hydrologic changes
- Multisectoral trade-offs are exacerbated by strengthening monsoon and greater interannual variability

Supporting Information:
- Supporting Information S1

Correspondence to:
J. D. Quinn,
jdq8@cornell.edu

Citation:
Quinn, J. D., Reed, P. M., Giuliani, M., Castelletti, A., Oyler, J. W., & Nicholas, R. E. (2018). Exploring how changing monsoonal dynamics and human pressures challenge multireservoir management for flood protection, hydropower production, and agricultural water supply. *Water Resources Research*, *54*. https://doi.org/10.1029/2018WR022743

Received 9 FEB 2018
Accepted 27 MAY 2018
Accepted article online 6 JUN 2018

©2018. American Geophysical Union. All Rights Reserved.

Exploring How Changing Monsoonal Dynamics and Human Pressures Challenge Multireservoir Management for Flood Protection, Hydropower Production, and Agricultural Water Supply

J. D. Quinn[1], P. M. Reed[1], M. Giuliani[2], A. Castelletti[2,3], J. W. Oyler[4], and R. E. Nicholas[4]

[1]Department of Civil and Environmental Engineering, Cornell University, Ithaca, NY, USA, [2]Department of Electronics, Information, and Bioengineering, Politecnico di Milano, Milano, Italy, [3]Institute of Environmental Engineering, ETH Zurich, Zurich, Switzerland, [4]Earth and Environmental Systems Institute, The Pennsylvania State University, University Park, PA, USA

Abstract Multireservoir systems require robust and adaptive control policies capable of managing hydroclimatic variability and human demands across a range of time scales. This is especially true for river basins with high intraannual and interannual variability, such as monsoonal systems that need to buffer against seasonal droughts while also managing extreme floods. Moreover, the timing, intensity, duration, and frequency of these hydrologic extremes may evolve with deeply uncertain changes in socioeconomic and climatic pressures. This study contributes an innovative method for exploring how possible changes in the timing and magnitude of the monsoonal cycle impact the robustness of reservoir operating policies designed assuming stationary hydrologic and socioeconomic conditions. We illustrate this analysis on the Red River basin in Vietnam, where reservoirs and dams serve as important sources of hydropower production, multisectoral water supply, and flood protection for the capital city of Hanoi. Applying our scenario discovery approach, we find that reservoir operations designed assuming stationarity provide robust hydropower performance in the Red River but that increased mean streamflow, amplification of the within-year monsoonal cycle, and increased interannual variability all threaten their ability to manage flood risk. Additionally, increased agricultural water demands can only be tolerated if they are accompanied by greater mean flow, exacerbating food-flood trade-offs in the basin. These findings highlight the importance of exploring the impacts of a wide range of deeply uncertain socioeconomic and hydrologic factors when evaluating system robustness in monsoonal river basins, considering in particular both lower-order moments of annual streamflow and intraannual monsoonal behavior.

1. Introduction

Designing robust management strategies for multipurpose reservoir systems requires a careful exploration of the capacity of alternative management plans to handle uncertain changes in climatic and human pressures over multiple time scales. From extreme precipitation events to prolonged drought, and rapid urbanization to intensive agriculture, a range of stochastic and potentially nonstationary climatic and anthropogenic factors influence how river basin systems should be managed both now and in the future (Bouwer, 2000; Mach et al., 2014; Vörösmarty et al., 2000). These uncertainties are often considered "deep," meaning decision makers possess discordant beliefs about what are appropriate prior probability distributions for their occurrence (Knight, 1921; Lempert et al., 2002).

In deeply uncertain decision contexts, Dessai et al. (2009) highlight the deficiencies of classical "predict-then-act" risk-based assessments, since both likelihoods and consequences are poorly defined. Instead, they advocate for "bottom-up" approaches in which exploratory modeling techniques (Bankes, 1993) are employed to discover robust strategies that perform well across a broad range of possible system conditions and external forcings, regardless of their likelihood. These methods, reviewed in several recent papers (Dittrich et al., 2016; Herman et al., 2015; Maier et al., 2016) include decision scaling (Brown et al., 2012; Poff et al., 2015), robust decision making (RDM; Lempert et al., 2003), and many-objective robust decision making (MORDM; Kasprzyk et al., 2013). Despite their methodological differences in implementation,

these approaches share two common goals: (i) to discover management plans that are robust to deep uncertainties in system conditions and external forcings and (ii) to discover scenarios under which these plans can no longer satisfy system goals and therefore need to be redesigned.

Recent research in the robustness literature has focused on the second of these goals, using the scenario discovery process to inform the design of Dynamic Adaptive Policy Pathways (DAPP; Haasnoot et al., 2013) in which decision makers monitor *signposts* of change that trigger the adoption of different policies when some critical value, or *adaptation tipping point* (Kwadijk et al., 2010), has been observed. Central to this method is the design of the signposts (i.e., factors monitored to estimate the system trajectory) and tipping points (i.e., values of the signposts that trigger policy changes). A broad range of candidate factors may be suitable, but discovering effective signposts is a challenging information selection problem (e.g., see discussions in Galelli & Castelletti, 2013; Galelli et al., 2014; Hermans et al., 2017). For example, Herman and Giuliani (2018) find that even monotonically trending hydrologic conditions may not be informative for management. In designing adaptive reservoir operations for Folsom Dam in California, they find that a 50-year moving average of annual streamflow is not informative for controlling floods since floods are primarily driven by shorter time scale events. However, they find that a 50-year moving average of the water-year centroid is informative, suggesting that seasonality changes may be more important for management.

One promising way to discover effective signposts and tipping points is by combining the DAPP approach with bottom-up exploratory modeling techniques such as RDM in which sensitivity analysis is performed to identify conditions under which current management plans fail (see e.g., Groves et al., 2014). However, in order to effectively combine these approaches, it is important to ensure that the scenarios sampled in the exploratory analysis adequately capture the system dynamics that might emerge under alternative climatic and socioeconomic futures (Pruyt & Islam, 2016). In particular, as noted by Herman and Giuliani (2018), simply sampling changes in mean hydroclimatic conditions may not be sufficient, especially given that changes in climate variability affect the frequency of extreme climate events more than changes in the mean (Katz & Brown, 1992). Changes in intraannual variability may also pose challenges, particularly for monsoonal systems for which water management strategies must balance competing concerns of flood protection in the wet season and drought management in the dry season.

Evaluating the effects of changes in the seasonality of monsoonal systems may be particularly important due to uncertainty in how climate change will affect wet versus dry season precipitation. With respect to the monsoon season in Southeast Asia, severe floods typically occur during La Niña (cold phase) conditions, while eastward shifts of the Walker circulation in the tropical Pacific Ocean during El Niño (warm phase) conditions reduce precipitation over the South China Sea, leading to prolonged droughts (Juneng & Tangang, 2005; Räsänen & Kummu, 2013; Shen & Lau, 1995; Wang et al., 2001; Xu et al., 2004). Given global warming will likely increase the incidence of the warm phase of El Niño Southern Oscillations (ENSO; Cai et al., 2014; Timmermann et al., 1999), one might therefore expect an increased frequency of drought conditions in the region in the future. However, Huijun (2002) and Jiang et al. (2004) find instability in the relationship between ENSO and monsoonal precipitation in Southeast Asia over both reanalysis data from the National Centers for Environmental Prediction and National Center for Atmospheric Research (NCAR) reanalysis project (Huijun, 2002), and simulations from an atmosphere-ocean general circulation model (Jiang et al., 2004). This instability has been attributed to shifts in the time of year in which sea surface temperature (SST) maxima occur in the tropical Pacific (Kane, 1999; Singhrattna et al., 2005), as well as in the location of SST maxima, with weaker monsoons occurring during the cold phase when the Intertropical Convergence Zone (ITCZ) tends to move southward as it does during El Niño years (Yancheva et al., 2007).

These shifting relationships have led to disagreement over whether the East Asian monsoon has and will continue to strengthen or weaken with climate change. A weakening of the East Asian monsoon since the 1920s has been observed in wind speeds over China and sea level pressure gradients (Guo et al., 2011; Jiang et al., 2010; Vautard et al., 2010; Zhou et al., 2009); however, Hsu et al. (2011) and Wang et al. (2012) observe increased precipitation since 1979 under an alternative definition of monsoon area, leading the Intergovernmental Panel on Climate Change (IPCC) Fifth Assessment Report (Hartmann et al., 2013) to place low confidence in the projection that the monsoon will weaken. Furthermore, more than 85% of the Coupled Model Intercomparison Project 5 (CMIP5) models predict an increase in mean precipitation in the East Asian summer monsoons (Hijioka et al., 2014). This projection does not extend to the dry season, though. Ray et al. (2015) find that general circulation models (GCMs) consistently project wetter South Asian monsoons but do not agree

on the sign of dry season precipitation, suggesting there may be shifts in seasonality. This hypothesis is supported by paleodata from sediment records in the South China Sea, which show an inverse correlation in the strengths of the winter and summer monsoon in Southeast Asia (Wang et al., 1999; Yancheva et al., 2007). When the ITCZ moves northward, the summer monsoon tends to strengthen, while the winter monsoon tends to weaken (Yancheva et al., 2007). Such seasonal shifts could also occur due to human behavior, as has been the focus of a vast body of literature on anthropogenic flow alteration (Kroll et al., 2015; Poff & Zimmerman, 2010; Richter et al., 1996; Vogel et al., 2007).

Despite these observations, prior bottom-up assessments in monsoonal systems have only explored the impacts of constant mean shifts in precipitation and temperature on water systems management (Ray et al., 2018; Yang et al., 2016). While exploring changes in seasonality is common in top-down climate assessments through the application of time and quantile-varying change factors (Anandhi et al., 2011; Diaz-Nieto & Wilby, 2005), to our knowledge, only Nazemi et al. (2013) have used bottom-up methods to investigate how changes in seasonality might influence the robustness of alternative water management strategies. Their analysis focused specifically on assessing the effects of changes in the timing of snowmelt, while we are interested in studying the effects of changes in both the timing and intensity of the monsoon. Bottom-up climate assessments of such seasonal changes could be performed by applying different change factors to different fragments of the historical annual cycle as in top-down assessments, but this could become cumbersome if a large number of fragments are needed to effectively capture the annual cycle.

In this study, we attempt to better capture the water management implications of potential changes in monsoonal dynamics through a simpler but expansive sampling of how the timing and magnitude of monsoonal seasonal extremes may evolve under a changing climate. We illustrate our contributions using the Red River basin in Southeast Asia, where four major reservoirs on the Vietnamese side of the basin serve multiple system objectives related to energy and water supply, as well as flood protection. Using a limited number of statistical parameters to describe streamflows and demands, we explore how a wide range of potential changes in both monsoonal flow regimes and socioeconomic conditions influence the performance of alternative multireservoir operating policies for the basin. Importantly, we not only analyze the effects of hydrologic shifts in the first two moments of annual streamflow but also intraannual variability. We then use logistic regression to define failure regions in which multireservoir operating policies designed for stationary conditions can no longer attain satisfactory performance. The combinations of interacting hydrologic and socioeconomic factors defining the failure regions can be used to design more robust operating policies in future analyses by serving as signposts for adaptive management plans.

Our paper is organized as follows. Section 2 provides a brief background of the Red River water systems management model. Section 3 describes the reservoir optimization model and subsequent scenario discovery experiment for sampling potential changes in monsoonal dynamics and human pressures. Section 4 presents the results of this analysis and discusses the broader implications of our findings for multiobjective reservoir management in monsoonal systems. Finally, Section 5 concludes with a summary of our key findings and opportunities for future work.

2. Multiobjective Water Systems Management Model

2.1. Red River Basin

The Red River basin is a monsoonal river system in Southeast Asia that flows from China and the Lao People's Democratic Republic through Vietnam to the Vietnamese East Sea. Just over half of the basin's 169,000 km^2 lie in Vietnam, making it the second largest river basin in the country to the Mekong. During the monsoon, the Red River serves as a vital agricultural resource to Vietnam, the second largest exporter of rice in the world (Yu et al., 2010). However, monsoonal rains also put the delta and capital city of Hanoi at risk of severe flooding. Several historical floods have devastated the delta region (Le Ngo et al., 2008), causing average annual damages of 130 million USD (Hansson & Ekenberg, 2002). Within the last 40 years, efforts have been made by the government to reduce flood risk by constructing reservoirs upstream of Hanoi. These reservoirs have also enabled greater water supply for agriculture during the dry season and hydropower production year-round. With 70% of the Vietnamese population of 93 million people employed in agriculture (Nguyen et al., 2002), and 46% of the country's installed electric power capacity in hydropower (Asian Development Bank, 2016), reservoirs have played an integral role in developing the local economy.

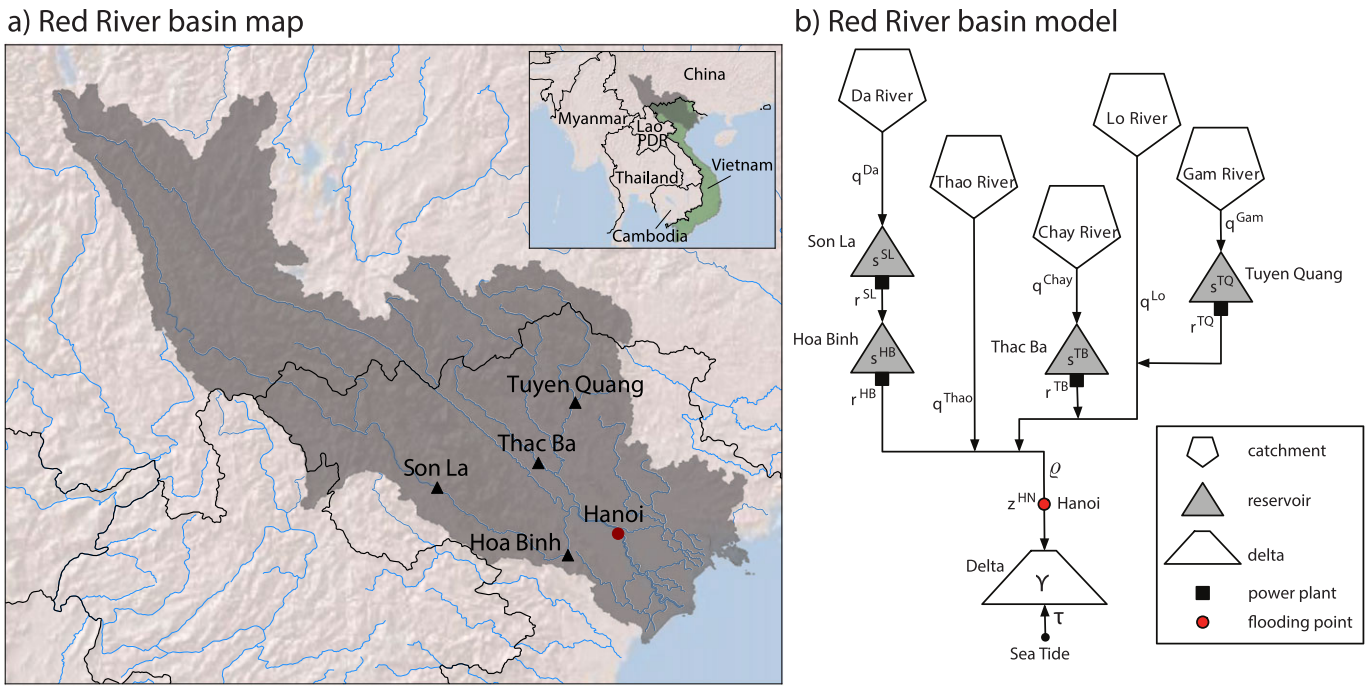

Figure 1. Map of the Red River basin (panel a) and schematization of the main components of the Red River basin model (panel b), reproduced from Quinn et al. (2017). Flows to each of the reservoirs shown in panel b are generated synthetically, releases from the reservoirs are determined by operating policies discovered through multiobjective optimization, and flows through the delta are modeled by a dynamic emulator of a MIKE 11 model of the downstream hydraulics.

However, while reservoirs provide flood protection, more consistent water supply and a source of electric power, conflicting operations favor each of these demands. Flood protection requires low reservoir levels to contain large flow events, while hydropower production and irrigation supply require high levels to enable a large head differential for energy generation and to buffer against drought. Furthermore, agricultural releases during the dry season conflict with the need to maintain high head for hydropower production. Consequently, designing operating policies for the multireservoir Red River system is a challenging multiobjective control problem (Giuliani et al., 2017). Compounding this challenge are many sources of uncertainty, such as how hydrologic conditions will evolve in a changing climate or how economic development will impact future water demands. In the context of hydrologic pressures, streamflow in the Red River is dominated by the annual monsoon from May to October, which in 6 months provides nearly 80% of the total annual flow. Yet as noted in the introduction, there is deep uncertainty in how the monsoon will be affected by climate change. In the context of socioeconomic pressures, water demand in the basin is currently dominated by agriculture, followed by aquaculture. However, total rice growing area in Vietnam has been declining recently due to rapid urbanization (Yu et al., 2010), suggesting there may be a shift in sectoral demand in the future. Building off of prior work in the Red River basin, we apply the MORDM (Kasprzyk et al., 2013) framework, described in section 3.1, to evaluate the robustness of candidate operating policies to these deep uncertainties.

2.2. Model Description

In this study, we employ the same water systems simulation model used by Giuliani et al. (2017) and Quinn et al. (2017) to optimize multiobjective operating policies for the four largest reservoirs in the Red River basin. Figure 1, reproduced from Quinn et al. (2017), shows the locations of these four reservoirs within the basin (panel a) as well as a schematic of the system model (panel b). Son La (SL) and Hoa Binh (HB), the two largest reservoirs, are located in series on the Da River, the largest tributary in the basin. Thac Ba (TB) and Tuyen Quang (TQ), two smaller reservoirs, are located in parallel on the Chay and Gam rivers, respectively. Altogether, these reservoirs have a total storage capacity of 22.67 billion m^3 and a power capacity of 4,782 MW.

The model illustrated in Figure 1b is composed of an upstream and a downstream component, each of which runs on a daily time step. The upstream model consists of synthetically generated daily flows on each of the five system tributaries (q_t^{Da}, q_t^{Thao}, q_t^{Chay}, q_t^{Lo}, q_t^{Gam}) and daily releases from each of the reservoirs

(r_t^{SL}, r_t^{HB}, r_t^{TB}, r_t^{TQ}). Monthly flows on each tributary are generated synthetically using Cholesky decomposition of resampled historical monthly flows and then disaggregated to daily flows using a nearest neighbor approach introduced by Nowak et al. (2010), in which daily flows from a probabilistically selected month in the historical record are proportionally scaled to match the synthetic monthly total. The Cholesky decomposition preserves temporal correlation within each flow series, while resampling the same historical flows at each site preserves spatial correlation across them (Herman et al., 2016; Kirsch et al., 2013). The generator was built to 51 years of historical flows from 1960 to 2010, and validation of its performance can be found in the supporting information to Quinn et al. (2017).

The synthetic flows on the Da, Chay, and Gam Rivers feed into the Son La, Thac Ba, and Tuyen Quang reservoirs. Releases from these reservoirs and Hoa Binh are determined by optimized operating policies, described in section 3.2. The releases from each of the reservoirs determine their daily hydropower production, which is modeled for each reservoir by an artificial neural network (ANN) mapping the kth reservoir's storage at the beginning of the time interval $[t, t+1)$, s_t^k, and release at the end of the time interval $[t, t+1)$, r_{t+1}^k, to production: $\eta_{t+1}^k = f(s_t^k, r_{t+1}^k)$. The releases feed into the downstream system model that consists of three additional ANNs used to approximate the outputs from a MIKE 11 hydraulic model while speeding up the computational time for optimization. The ANNS, built to a 62-year simulation of daily routing in the delta, estimate the daily water volume in the delta's irrigation canals, Υ_t, the water level at Hanoi, z_t^{HN}, and the water supply deficit, D_t, which is a function of Υ_t (Dinh, 2015). The water supply deficit is a function of the volume of water in the canals because this water is used to both supply water for irrigation and municipal and industrial demands and to ensure sufficient instream flows for fisheries in the delta. All data used to build the Red River model are from the Ministry of Agriculture and Rural Development (MARD) of Vietnam and were collected during the Integrated and sustainable water Management of Red Thai Binh Rivers system in changing climate (IMRR) project (http://xake.elet.polimi.it/imrr/).

3. Methods

3.1. Multiobjective Optimization and Robustness Analysis

The primary goal of this study is to introduce a method for exploring how changing monsoonal dynamics and human pressures challenge multireservoir management of multisectoral trade-offs in monsoonal river basins. In applying this method to the Red River basin, we (i) discover robust operating policies for the system's reservoirs and (ii) determine the most important hydrologic and socioeconomic drivers of their performance in order to inform adaptive management strategies, for example, by setting triggers for reoperations or by incentivizing demand management. Many different strategies have been proposed in the literature for defining and evaluating robustness; however, as Herman et al. (2015) highlight in their taxonomy of robustness frameworks, these approaches all share four common components. Figure 2, adapted from Herman et al. (2015), illustrates how these four components, and an additional fifth, are applied in this particular study.

The first component is the selection of decision alternatives, in this case, alternative reservoir operating policies (Figure 2, Box I). Following the MORDM framework introduced by Kasprzyk et al. (2013), we discover nondominated operational alternatives through multiobjective optimization (described in section 3.2), considering only well-characterized, stationary streamflow uncertainty in the optimization.

The second component of our robustness analysis is to evaluate the decision alternatives in different states of the world (SOWs) that could pose operational challenges in the future (Figure 2, Box II). In this study, we discover the most important factors by generating alternative SOWs through a design of experiments, focusing specifically on hydrologic and socioeconomic drivers. A core contribution of this study includes the use of synthetic streamflow generation to capture a diverse suite of nonstationary monsoonal dynamics. Our approach for generating SOWs is described in detail in section 3.3.

After reevaluating the Red River system's candidate control policies in different SOWs, we utilize robustness measures to rank the alternatives and inform further vulnerability assessments using scenario discovery (Figure 2, Box III). Here we calculate a satisficing metric (Starr, 1969) for each design alternative representing the percent of sampled worlds in which minimum performance levels across the system objectives are met. The results of our robustness analysis are provided in section 4.1.

Next, we employ sensitivity analysis to discover which conditions sampled in the scenario generation process control the robustness of different design alternatives (Figure 2, Box IV). Here we discover scenarios of concern

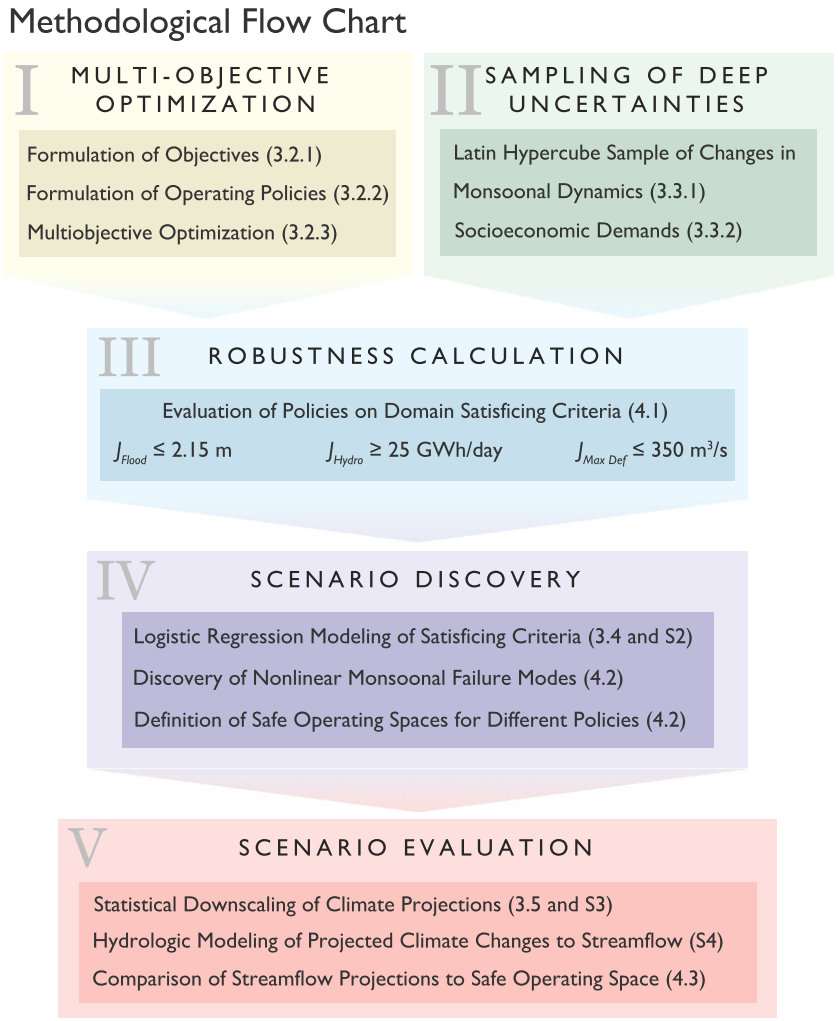

Figure 2. Methodological flow chart of how we assess robustness in this study and the sections of the paper in which each step is presented. See the main text for further description.

using logistic regression, described in sections 3.4 and supporting information S2. The results of this analysis, presented in section 4.2, could be used in future work to inform when policies should be redesigned (Groves et al., 2014) or when controlling factors should be managed to mitigate their negative effects (see, e.g., Herman et al., 2014).

Finally, we evaluate the plausibility that scenarios discovered to be of concern might occur in the future (Figure 2, Box V). While not mentioned as an explicit step in the robustness taxonomy of Herman et al. (2015), this step is often added to climate change studies to see where projections from GCMs fall relative to the scenarios of concern (Brown et al., 2012; Herman et al., 2016; Steinschneider, McCrary, Wi et al., 2015; Whateley et al., 2014). This scenario evaluation step is described in sections 3.5 and supporting information S3–S4, and the results of the analysis are presented in section 4.3.

3.2. Problem Formulation

Quinn et al. (2017) analyzed several rival framings for how the multiobjective Red River control problem should be formulated to best capture stakeholder objectives and preferences. Insights from that study were used to design the problem formulation described here, which is intended to capture the risk aversion of Vietnamese stakeholders with respect to extreme floods and droughts. Reservoir operating policies optimized to this formulation will inform guidelines being developed by the Vietnamese government. To optimize reservoir operating policies for the Red River, we use Evolutionary Multiobjective Direct Policy Search (EMODPS; Giuliani et al., 2016). This method uses multiobjective evolutionary algorithms (MOEAs) to discover nondom-

inated parameterizations of operating policies that optimize system performance over multiple objectives computed during simulation with these policies. To allow for flexible operating behavior, nonlinear approximating networks are used to describe the reservoir operating policies.

3.2.1. Formulation of Objectives

In this study, candidate operating policies are simulated over N stochastic ensembles of T year simulations in which the dth objective, J_d, is quantified according to equation (1):

$$J_d = \Psi_{i\in(1,\ldots,N)}\left[\Phi_{t\in(1,\ldots,365T)}\left[g_d(t,i)\right],\right] \tag{1}$$

where $g_d(t,i)$ is the value of the dth objective on day t in the ith ensemble member, Φ is an operator for the aggregation of $g_d(t,i)$ over T years (such as the sum, $\sum$), and Ψ is a statistic used to filter the noise across the N ensemble members (such as the expected value, $\mathbb{E}$). Here we simulate policies over a 1,000-year sequence of stochastic streamflows that we divide into $N = 1{,}000$ consecutive ensemble members of $T = 1$-year simulations to compute the objectives. Generating consecutive years ensures that the distribution of initial conditions for the ensemble members is representative of those obtained by the control strategy being simulated.

The first system goal in this study is to minimize J_{Flood}, a measure of flooding. We quantify this objective as the amount by which the annual maximum water level at Hanoi exceeds 11.25 m in the worst first percentile year. This stage is an alarm level elicited from stakeholders. We constrain J_{Flood} to be less than 2.15 m, the difference between 11.25 m and the dike height of 13.4 m, ensuring protection to the 100-year flood. This objective is therefore calculated by letting $g_{\text{Flood}}(t,i) = z^{HN}_{t,i}$, where $z^{HN}_{t,i}$ is the water level at Hanoi on day t of the ith ensemble member, $\Phi = \max_{365T}$ and $\Psi = \text{quantile}_N\{\Phi, 0.99\}$.

The second system goal is to maximize J_{Hydro}, a measure of hydropower production. We compute this objective as the average daily production within each ensemble member and again maximize the worst first percentile across the ensemble, so $g_{\text{Hydro}}(t,i) = \sum_k \eta^k_{t,i}$, where $\eta^k_{t,i}$ is the energy production from reservoir k on day t of the ith ensemble member, $\Phi = \mathbb{E}_{365T}$ and $\Psi = \text{quantile}_N\{\Phi, 0.01\}$. We maximize production rather than revenue because energy is sold by the government at a fixed rate, so these measures are equivalent. Since markets and prices may change in the future, alternative formulations could be tested in subsequent analyses, but here we focus solely on analyzing the sensitivity of total production to uncertainties in system conditions and external forcings.

The final system goal is to minimize J_{Deficit^2}, a measure of the water supply deficit. For this objective, we compute the average daily squared deficit and minimize the worst first percentile across the ensemble, so $g_{\text{Deficit}^2}(t,i) = D^2_{t,i}$, where $D^2_{t,i}$ is the squared deficit on day t of the ith ensemble member, $\Phi = \mathbb{E}_{365T}$ and $\Psi = \text{quantile}_N\{\Phi, 0.99\}$. Daily deficits are squared to numerically favor frequent but small deficits over less frequent, more severe deficits.

Combining all of these objectives, the goal of the multiobjective Red River control problem is to find nondominated parameter sets θ^* minimizing the three objectives. This is defined formally by equations (2)–(7):

$$\theta^* = \text{argmin}_\theta J(\theta), \tag{2}$$

where

$$J = \begin{bmatrix} -J_{\text{Hydro}}(\theta) \\ J_{\text{Deficit}^2}(\theta) \\ J_{\text{Flood}}(\theta) \end{bmatrix}, \tag{3}$$

$$J_{\text{Flood}} = \text{quantile}_N\left\{\max_{365T}\left(z^{HN}_{t,i}\right), 0.99\right\}, \tag{4}$$

$$J_{\text{Deficit}^2} = \text{quantile}_N\left\{\mathbb{E}_{365T}\left(D^2_{t,i}\right), 0.99\right\}, \tag{5}$$

$$J_{\text{Hydro}} = \text{quantile}_N\left\{\mathbb{E}_{365T}\left(\sum_k \eta^k_{t,i}\right), 0.01\right\}, \tag{6}$$

subject to

$$J_{\text{Flood}}(\theta) \leq 2.15, \tag{7}$$

where θ is a vector of parameters describing the operating policies defined in section 3.2.2. These parameters therefore serve as the decision variables optimized by the MOEA.

3.2.2. Formulation of Operating Policies

In this study, operating policies for each of the four reservoirs are determined by Gaussian radial basis functions (RBFs) mapping a vector of system states to reservoir releases. Gaussian RBFs have been shown to provide effective operating policies in this system, generalizing better to out-of-sample streamflows than policies represented by ANNs with hyperbolic tangent activation functions (Giuliani et al., 2016). The RBF representation of daily release policies at each reservoir is given by equation (8):

$$u_t^k = \sum_{i=1}^{A} w_i^k \exp\left(- \sum_{j=1}^{B} \frac{\left((x_t)_j - c_{j,i}\right)^2}{b_{j,i}^2} \right), \tag{8}$$

where u_t^k is the policy-prescribed release from the kth reservoir on day t (normalized on [0,1]); $(x_t)_j$ is the value of the jth input at time t (normalized on [0,1]); A is the number of RBFs; B the number of inputs; and w_i^k , $c_{i,j}$, and $b_{i,j}$ are the weights, centers, and radii, respectively, of the ith RBF associated with the kth reservoir and jth input. The actual release at the kth reservoir at the end of the time interval $[t, t + 1)$, r_{t+1}^k, is equal to the unnormalized value of u_t^k unless physical constraints prohibit it (e.g., if the prescribed release lies outside the minimum and maximum allowable releases, if there is insufficient water to meet the prescribed release, or if the prescribed release would result in the reservoir storage capacity being exceeded).

As defined in equations (2)–(7) in section 3.2.1, the goal of EMODPS is to find a nondominated set of parameter vectors θ^* minimizing the system objectives. The parameter vector θ is composed of the weights, centers, and radii defining the RBF policies, that is, $\theta = [w_i^k, c_{i,j}, b_{i,j}]$ where $i = \{1, \ldots, A\}$, $j = \{1, \ldots, B\}$, and $k = \{1, \ldots, K\}$. In this study, $K = 4$ for the four reservoirs and $w_i^k \in [0, 1]$, $c_{i,j} \in [-1, 1]$, and $b_{i,j} \in (0, 1]$. This results in a total of $A(K + 2B)$ parameters. We use $A = 11$ RBFs and $B = 6$ inputs: the storage at each of the four reservoirs and a cyclic representation of time with phase-shifted sin(·) and cos(·) functions, that is, $\mathbf{x_t} = \left[s_t^{SL}, s_t^{HB}, s_t^{TB}, s_t^{TQ}, \sin\left(\frac{2\pi t}{365} - p_1\right), \cos\left(\frac{2\pi t}{365} - p_2\right) \right]$ where p_1 and p_2 are phase shifts on $[0, 2\pi]$. For the sin(·) and cos(·) functions, we also set their associated centers to 0 and radii to 1 since the intent of these parameters is to horizontally translate and scale the inputs, but outside of sin(·) and cos(·) functions they would be vertically translating them. We instead include phase shifts within the sin(·) and cos(·) functions to serve as centers in horizontally translating the inputs but do not include a scale parameter, as this would result in them no longer being full period over the year. Given the above changes, the RBF representation of the policies in this paper can be described by equation (9):

$$u_t^k = \sum_{i=1}^{A} w_i^k \exp\left(- \left[\sum_{j=1}^{B-2} \frac{\left((x_t)_j - c_{j,i}\right)^2}{b_{j,i}^2} + (x_t)_{B-1}^2 + (x_t)_B^2 \right] \right), \tag{9}$$

where $(x_t)_{B-1} = \sin\left(\frac{2\pi t}{365} - p_1\right)$ and $(x_t)_B = \cos\left(\frac{2\pi t}{365} - p_2\right)$. It should be noted that since all inputs are normalized on [0,1], squaring the sin(·) and cos(·) functions in equation (9) does not create two separate cycles per year. The total number of parameters to be optimized in this formulation is $A(K + 2(B - 2)) + 2 = 134$.

3.2.3. Multiobjective Optimization

As stated in section 3.2, EMODPS exploits MOEAs to optimize the parameter vector θ defining the multireservoir control policies in order to minimize multiple objectives computed over the system simulation. Given recent documented success of the multimaster Borg MOEA in optimizing operating policies for complex reservoir control problems (Giuliani et al., 2017; Zatarain Salazar et al., 2017), we use this algorithm to identify Pareto-approximate operating policies for the Red River's four largest reservoirs. Multimaster Borg is a hierarchically parallelized version of the Borg MOEA (Hadka & Reed, 2013) that allows communication across multiple master-worker parallel implementations of the Borg algorithm. This communication has been shown to improve the algorithm's reliability across random seed trials, improving performance of the worst seeds without degrading performance of the best seeds (Giuliani et al., 2017; Hadka & Reed, 2015; Zatarain Salazar et al., 2017). The Borg algorithm requires that users specify "epsilons," or significant levels of precision below which they are impartial to differences in performance, for each objective. Consistent with prior work in the basin (Giuliani et al., 2017; Quinn et al., 2017), we use epsilons of 0.05 for J_{Flood}, 25.0 for J_{Deficit^2}, and 0.5 for J_{Hydro}

and run the multimaster Borg with five seeds using a 16-master implementation with 400,000 function evaluations allocated to each master. The optimization was performed on the Texas Advanced Computing Center (https://www.tacc.utexas.edu/stampede/) using 512 cores per island for a total of 400,000 computational hours. Visual inspection of search progress indicated the algorithm had converged, with little variability across seeds.

3.3. Sampling of Deep Uncertainties

Here we explain how we evaluate the effects of monsoonal changes (section 3.3.1) and evolving socioeconomic demands (section 3.3.2) on the ability of optimized Red River control policies to attain satisfactory performance. This analysis provides a means of identifying tolerable windows of change as well as conditions that should trigger reoperation of the Red River reservoirs. Since hydropower production, flood risk, and nonagricultural water demands are affected directly by streamflow, and agricultural water demands are influenced not only by the climate but also human decisions regarding what crops to plant in what quantities, we directly generate synthetic streamflows and multisectoral water demands for this scenario discovery analysis.

3.3.1. Monsoonal Dynamics

The main streamflow characteristics that we consider in our scenario discovery experiment are the log-space annual mean and standard deviation, as well as intraannual flow variability tied to the monsoon. These characteristics are of concern for several reasons: There is great uncertainty in the direction of mean changes in precipitation in East Asia, interannual variability is expected to increase globally, and it is unclear how the monsoon will be affected by climate change (Hijioka et al., 2014). To alter these flow characteristics for our scenario discovery process, we first generate a series of synthetic streamflows built to stationary conditions and then rescale them to produce the desired effects. Although in this study we generate synthetic flows as described in section 2.2, our exploratory sampling approach could be flexibly used with alternative synthetic streamflow generators (see reviews by Salas et al., 1980 and Hao & Singh, 2016 for examples).

The main goal of the rescaling process is to find a vector of monthly multipliers to apply to the stationary synthetic time series. For this process, consider two ensembles: $\mathbf{Q_S} \in \mathbb{R}^{N_S \times 12}$ of N_S years of synthetic monthly flows and $\mathbf{Q_H} \in \mathbb{R}^{N_H \times 12}$ of N_H years of historical monthly flows. We first perform a log-transform of each of these ensembles to formulate time series of normally distributed monthly flows, $\mathbf{Y_S} = \ln(\mathbf{Q_S})$ and $\mathbf{Y_H} = \ln(\mathbf{Q_H})$. We then standardize $\mathbf{Y_S}$ to generate ensembles of synthetic standard normal monthly flows, $\mathbf{Z_S}$, as shown in equation (10):

$$Z_{S_{i,j}} = \frac{Y_{S_{i,j}} - \hat{\mu}_j}{\hat{\sigma}_j}, \tag{10}$$

where $\hat{\mu}_j$ and $\hat{\sigma}_j$ are the sample mean and standard deviation of the jth month's log-transformed flows from $\mathbf{Y_H}$. To rescale the stationary synthetic monthly streamflows $\mathbf{Q}_S$ into alternative streamflow scenarios $\mathbf{Q'_S}$, vectors of monthly varying mean multipliers $\mathbf{M}_\mu = [M_{\mu,1}, \ldots, M_{\mu,12}]$ and standard deviation multipliers $\mathbf{M}_\sigma = [M_{\sigma,1}, \ldots, M_{\sigma,12}]$ are applied to $\hat{\mu}_j$ and $\hat{\sigma}_j$, respectively, when back-transforming Z_S, as shown in equation (11):

$$Q'_{S_{i,j}} = \exp\left(M_{\mu,j}\hat{\mu}_j + M_{\sigma,j}\hat{\sigma}_j Z_{S_{i,j}}\right). \tag{11}$$

If only the log-space annual mean and standard deviation are changed, then all elements of $\mathbf{M}_\mu$ and $\mathbf{M}_\sigma$ are constant (i.e., $M_{\mu,i} = m_\mu \forall i$ and $M_{\sigma,i} = m_\sigma \forall i$, where m_μ and m_σ are constants). Once these multipliers have been applied to calculate $\mathbf{Q'_S}$, the adjusted monthly flows are disaggregated to daily flows according to the same proportions used to disaggregate the corresponding stationary monthly flows $\mathbf{Q_S}$ to daily flows.

Figure 3 shows the effects of the constant multipliers m_μ and m_σ on the flow durations curves (FDCs) of daily flows in the Da River, which provides about half of the Red River basin's flow. In panel a, the range spanned by stationary synthetic flows is shown in medium blue, while the range spanned by rescaled flows generated with a log-space mean multiplier of $m_\mu = 1.05$ is shown in dark blue and $m_\mu = 0.95$ in light blue. Because the multipliers are applied in log-space, these 5% increases and decreases can yield fairly large differences in real-space flow magnitude. In panel b, the range of stationary synthetic flows is again shown in medium blue, while the range of rescaled flows generated with a log-space standard deviation multiplier of $m_\sigma = 1.5$ is shown in dark blue and $m_\sigma = 0.5$ in light blue. As one would expect, increasing the log-space annual standard

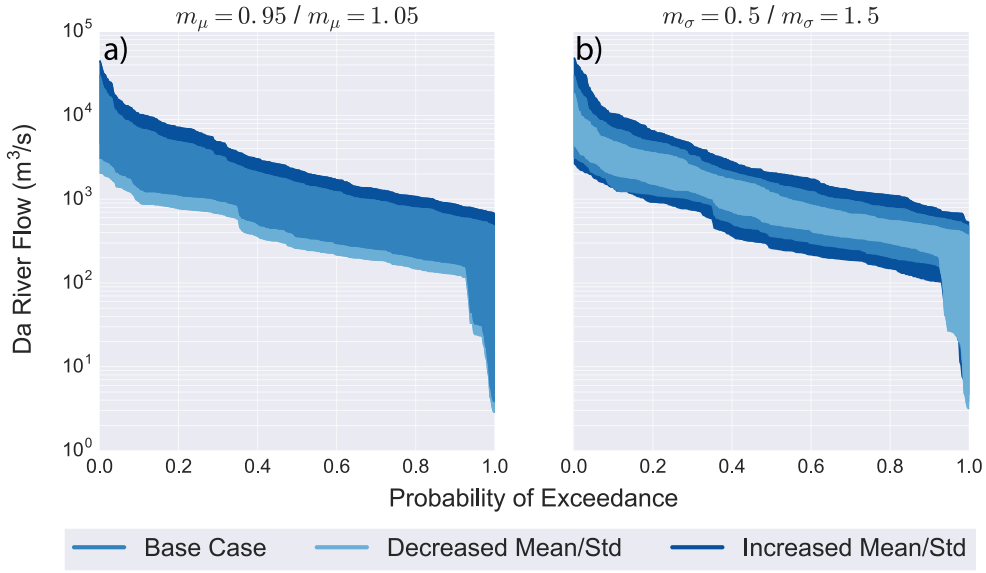

Figure 3. Ranges spanned by synthetically generated flow duration curves on the Da River under base case, that is, historical, conditions (medium blue) as well as increased (dark blue) or decreased (light blue) log-space annual mean (panel a) and annual standard deviation (panel b). The multipliers displayed are those spanned in our scenario discovery experiment.

deviation produces both wetter and drier years, while decreasing it reduces the range of generated flows. It should also be noted that increasing the log-space standard deviation also increases the real-space mean, greatly increasing flood risk.

To model solely monsoonal changes to the intraannual distribution of flows, we vary the elements of $\mathbf{M}_\mu$ cyclically in time but with no change to the log-space mean flow. This could be achieved by exploring the effects of separate change factors for each month, but that would require a large number of parameters for the sensitivity analysis. In order to model smooth, continuous changes in seasonality with a limited number of parameters, we instead fit Fourier series to the historical log-space monthly means and calculate time-varying multipliers by dividing the monthly means predicted by an adjusted harmonic, y_2, by those predicted by the historical fit, $\hat{y}_1$. This should be appropriate for monsoonal systems, since the hydrograph is dominated by the annual cycle (first harmonic), with additional harmonics allowing for asymmetric rising and falling limbs. We do not calculate different within-year multipliers for $\mathbf{M}_\sigma$, only $\mathbf{M}_\mu$, but future work could explore within-year changes to $\mathbf{M}_\sigma$ as well.

In this system, we find that the log-space mean monthly flows in each of the five Red River tributaries are modeled well by the first two harmonics (with R^2 values between 0.996 and 0.999 across the sites). That is, the log-space mean monthly flow, $\widehat{y_1(i)}$, at each site can be described by equation (12):

$$\widehat{y_1(i)} = \bar{y} + C_1 \cos\left(\frac{2\pi i}{12} - \phi_1\right) + C_2 \cos\left(\frac{2 \times 2\pi i}{12} - \phi_2\right), \tag{12}$$

where $\bar{y}$ is the mean of the historical time series of log-space monthly means, C_1 and ϕ_1 are the amplitude and phase, respectively, of the first harmonic (i.e., annual cycle), C_2 and ϕ_2 are the same for the second (i.e., semi-annual cycle), and i is the month of the year, from 1 for May (the beginning of the monsoon) to 12 for April (the end of the dry season). Assuming future streamflows will also be modeled well by equation (12), we create adjusted time series, y_2, for each site by applying multipliers to C_1 and/or C_2 and phase shifts to ϕ_1 and/or ϕ_2, thereby capturing changes in seasonality with only four parameters as opposed to 12 for 12 months. Increases in the amplitudes capture strengthening monsoons, while decreases capture weakening monsoons, and adjustments to the phase shifts capture changes in its timing. These parameters could also encompass changes in seasonality caused by upstream dam construction in China, highlighting that the cause may not matter, as long as water managers can track the effect.

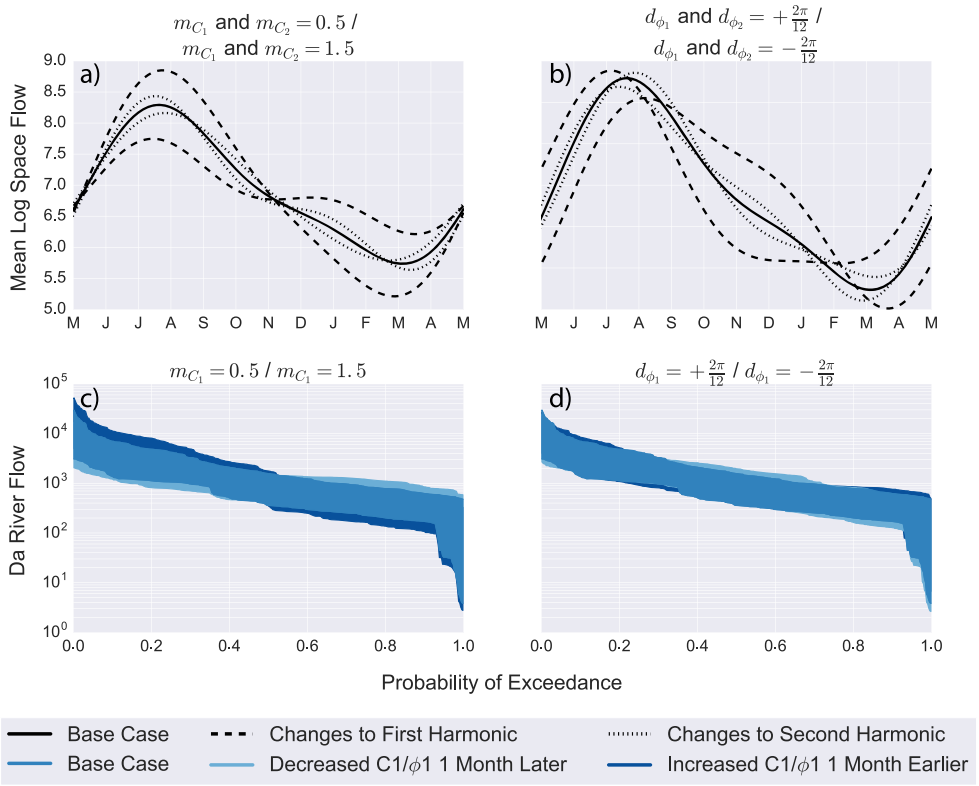

Figure 4. Effects of changes in the amplitude (panels a and c) and phase (panels b and d) of the first two harmonics on the log-space mean hydrographs (panels a and b) and flow duration curves (panels c and d) of the Da River. The multipliers displayed are those spanned in our scenario discovery experiment.

The amplitude multipliers, m_{C_1} and m_{C_2}, and phase shift deltas, d_{ϕ_1} and d_{ϕ_2}, are used to calculate a new cycle of mean monthly flows, y_2, according to equation (13):

$$y_2(i) = \bar{y} + m_{C_1} C_1 \cos\left(\frac{2\pi i}{12} - (\phi_1 - d_{\phi_1})\right) + m_{C_2} C_2 \cos\left(\frac{2 \times 2\pi i}{12} - (\phi_2 - d_{\phi_2})\right). \quad (13)$$

The ith element of $\mathbf{M}_\mu$ and $\mathbf{M}_\sigma$ can then be calculated as $y_2(i)/\widehat{y_1(i)}$. In order to change the log-space mean annual flow simultaneous to the intraannual distribution, the ith element of $\mathbf{M}_\mu$ can be calculated according to equation (14):

$$M_{\mu,i} = \left[m_\mu y_2(i)/\widehat{y_1(i)}\right], \quad (14)$$

Figure 4 illustrates the effects of m_{C_1}, m_{C_2}, d_{ϕ_1}, and d_{ϕ_2} on the log-space mean hydrographs and FDCs of the Da River. Panel a shows the historical fit, $\hat{y}_1$, with a solid black line and the effects on y_2 of setting $m_{C_1} = 1.5$ or $m_{C_1} = 0.5$ with dashed black lines and of setting $m_{C_2} = 1.5$ or $m_{C_2} = 0.5$ with dotted black lines. In both cases, when the multiplier is greater than 1, the peaks are higher and the troughs lower, and when the multiplier is less than 1, the reverse is true. Panel a shows that m_{C_1} has a much greater influence on the annual cycle than m_{C_2}. Moving to panel c, the effect of m_{C_1} on the Da River FDCs is illustrated. The range of base case FDCs is colored medium blue; the range when $m_{C_1} = 1.5$, dark blue; and when $m_{C_1} = 0.5$, light blue. Again, one can see that the highest flows become larger when $m_{C_1} = 1.5$ and the lowest flows smaller, while the reverse is true when $m_{C_1} = 0.5$. However, it should be noted that increases in monsoonal flows that occur without decreases in dry season flows can be modeled by combining changes to both the amplitude of the first harmonic and the log-space mean. It should also be noted that since these multipliers are applied in log-space, an increase in the amplitude of either harmonic will result in greater real-space increases in the monsoon season than decreases in the dry season, thereby increasing the real-space mean.

Panels b and d are similar to a and b, except they show the effects of d_{ϕ_1} and d_{ϕ_2} instead of m_{C_1} and m_{C_2}. In panel b, the historical mean fit, $\hat{y}_1$, is again shown with a solid black line, while the dashed lines show the

Table 1
Ranges of Hydrologic Factors Sampled in Our Scenario Discovery Analysis

Deeply uncertain factor	Lower bound	Upper bound	Change to hydrograph
Log-space mean multiplier, m_μ (–)	0.05	1.05	Decreases or increases all flows year-round
Log-space std multiplier, m_σ (–)	0.5	1.5	Decreases or increases interannual variability
Log-space C_1 multiplier, m_{C_1} (–)	0.5	1.5	Decreases or increases amplitude of annual monsoonal cycle
Log-space C_2 multiplier, m_{C_2} (–)	0.5	1.5	Decreases or increases amplitude of semiannual monsoonal cycle
Log-space ϕ_1 delta, d_{ϕ_1} (radians)	$-2\pi/12$	$+2\pi/12$	Shifts annual monsoonal cycle earlier or later
Log-space ϕ_2 delta, d_{ϕ_2} (radians)	$-2\pi/12$	$+2\pi/12$	Shifts semiannual monsoonal cycle earlier or later
Evaporation delta, d_e (mm/day)	−0.5	+1.0	Decreases or increases evaporation year-round

Note. States of the world are generated from a Latin hypercube sample across all hydrologic and socioeconomic factors, with each factor sampled uniformly within its bounds. However, since multipliers are applied in log-space, the samples are not uniform in real-space.

effect of $d_{\phi_1} = \pm 2\pi/12$ radians (1-month shift) and the dotted lines the effect of $d_{\phi_2} = \pm 2\pi/12$ radians. Again, changes in the first harmonic have much greater effects than changes in the second. Panel d shows the effects of changes in d_{ϕ_1} on the Da River FDCs, with the range of historical flows shown in medium blue, the range of flows with a leftward phase shift in dark blue, and with a rightward phase shift in light blue. In panel b, it can be seen that the leftward phase shift of d_{ϕ_1} results in a slightly higher peak in July instead of August and a higher trough in the dry season. These changes result in higher high and low flows in the FDCs in panel d. The rightward phase shift shows lower peaks and troughs in panel b, resulting in lower high and low flows in panel d but higher moderate flows due to a slower die-off in the monsoon. However, these changes in the FDCs are much less significant than those observed as a result of m_{C_1} in panel c.

The final hydrologic factor we adjust in our scenario discovery analysis is the evaporation rate. This rate influences the amount of water evaporated from the reservoirs, which reduces the total system storage. Increased evaporation could therefore potentially help reduce floods but at the cost of hydropower production and water supply for irrigation. We apply a delta shift to historical evaporation rates of d_e mm/day in our analysis. Table 1 summarizes the ranges of all hydrologic factors explored in our study.

3.3.2. Socioeconomic Demands

In addition to generating alternative scenarios for how hydrologic characteristics might change in the future, we also generate alternative demand scenarios to capture how evolving socioeconomic conditions might influence the robustness of alternative reservoir operating policies. We break the demand down into three primary sectors: agriculture, aquaculture, and other. We apply independent multipliers to each of these sectors: m_{ag} for agriculture, m_{aq} for aquaculture, and m_o for all other demands, sampling greater potential growth in other demands than agriculture and aquaculture due to urbanization. Figure 5a shows the historical distribution of these demands over time, while Figure 5b shows the effect of simultaneously sampling the upper and lower limits of m_{ag}, m_{aq}, and m_o to illustrate the full range of generated scenarios. We also sample a delta shift in the timing of total demand, d_D, from 30 days earlier to 30 days later, illustrated in Figure 5c. The ranges explored for each of these factor adjustments, informed by plausible changes assessed in Rossi (2016), are given in Table 2. In our experimental design, we generate a total of 1,000 alternative SOWs from a Latin hypercube sample across the factor ranges given in Tables 1 and 2, sampling all factors uniformly within their bounds. While many of these deeply uncertain factors may be correlated in reality, the goal of this experiment is simply to fill the space of plausible futures to identify SOWs in which current policies fail. Subsequent analysis considering correlations among different uncertain factors can then be used to assess whether or not these failure states may be likely. For example, if evaporation increases, agricultural demands will likely increase as well, so vulnerabilities associated with these common changes may be more concerning than vulnerabilities associated with likely independent changes, such as increased municipal demands and increased evaporation.

3.4. Scenario Discovery

After reevaluating the candidate operating policies generated from our multiobjective optimization on the alternative SOWs described in section 3.3, we calculate the robustness of each policy using a satisficing metric quantified as the percent of worlds in which $J_{\text{Flood}} \leq 2.15$ m (providing protection to the 100-year flood), $J_{\text{Hydro}} \geq 25$ GWh/day, and the worst first percentile of the maximum daily deficit is less than 350 m^3/s. We choose this formulation of the deficit criterion, called $J_{\text{Max Def}}$, because it is more intuitive than the worst first

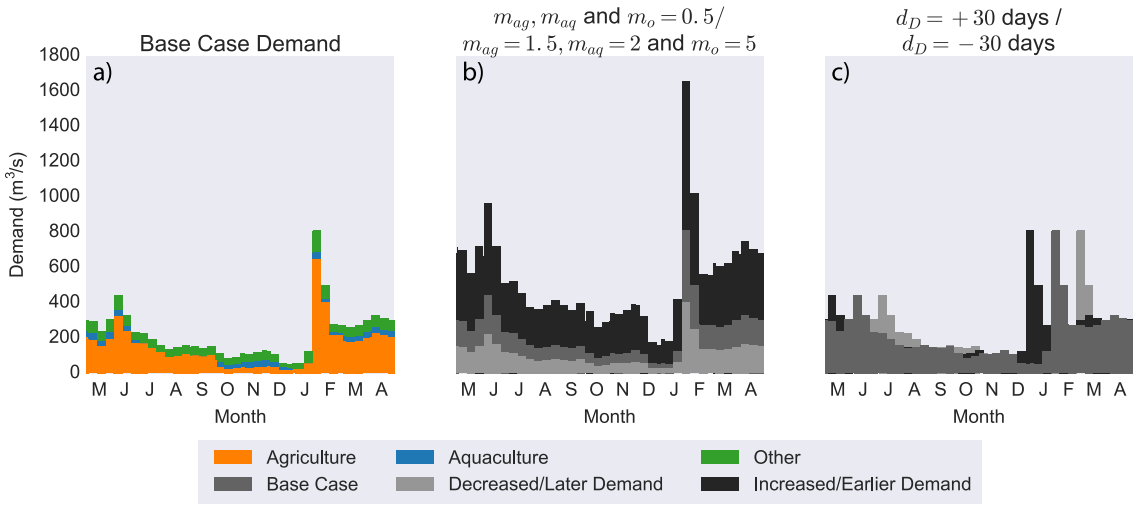

Figure 5. Base case distribution and timing of average water demand in the Red River basin across sectors (panel a), as well as the effects of changes in the amount (panel b) and timing (panel c) of sectoral demand. Panel a shows that most of the water demand is for agriculture (orange). The second largest sector is aquaculture, shown in blue. Demand from all other sectors, including industrial and municipal, is shown in green. In panels b and c, base case, that is, average historical conditions, are shown in medium gray, increased and earlier demand in black, and decreased and later demand in light gray. The multipliers displayed are those spanned in our scenario discovery experiment.

percentile of the average daily squared deficit. We still optimize to J_{Deficit^2} to minimize both high deficits and persistent low deficits but ensure the policies generalize well by evaluating their robustness on an objective to which they were not optimized. The results of our robustness analysis are presented in section 4.1.

After quantifying the robustness of each alternative operating policy, we select the most robust solution on each objective, as well as across objectives, for further analysis. We then use logistic regression to identify combinations of hydrologic and socioeconomic factors under which the selected policies fail to attain satisfactory performance. This allows us to model the probability that a given control policy is able to satisfy a particular performance criterion as a function of the deeply uncertain factors. While we may not know the probability that a given SOW will occur, we can use logistic regression to predict the probability that a policy will be able to meet satisfactory performance levels in that SOW, should it occur. Stakeholders can then divide the space of deeply uncertain factors into success and failure regions based on the probability with which they would like to satisfy different performance criteria. A detailed description of the logistic regression modeling is provided in section S2 of the supporting information. The results of the scenario discovery analysis are given in section 4.2.

3.5. Scenario Evaluation

The final step in our robustness analysis is to evaluate the plausibility of the hydrologic scenarios discovered to be of concern in section 4.2. We do this by driving a statistical hydrologic model with projected precipitation and temperature series from GCMs. Defining 1976–2005 as climatology within each projection, we reestimate the values of the streamflow factors determined to be most critical by the logistic regression over 30-year

Table 2
Ranges of Socioeconomic Factors Sampled in Our Scenario Discovery Analysis

Deeply uncertain factor	Lower bound	Upper bound
Agricultural demand multiplier, m_{ag} (–)	0.5	1.5
Aquaculture demand multiplier, m_{aq} (–)	0.5	2.0
Other demand multiplier, m_o (–)	0.5	5.0
Demand delta, d_D (days)	−30	+30

Note. States of the world are generated from a Latin hypercube sample across all hydrologic and socioeconomic factors, with each factor sampled uniformly within its bounds.

moving windows. This requires, first, downscaling precipitation and temperature projections to the Red River basin and, second, running them through a hydrologic model.

For the climate downscaling, we use projections from 34 GCMs in the CMIP5 multimodel ensemble from 18 different institutions, each run with multiple initial conditions across all four representative concentration pathways (RCPs). A list of all models is provided in Table S9 of the supporting information. Before downscaling, we bias correct the CMIP5 projections using the Asian Precipitation - Highly-Resolved Observational Data Integration Towards Evaluation (APHRODITE) observation data set (Yatagai et al., 2012) and a variation of the modified equidistant cumulative distribution function matching algorithm (EDCDFm; Li et al., 2010) developed by Pierce et al. (2015). EDCDFm is a quantile mapping approach that adjusts the model CDF based on value differences by quantile between the model and observations over an historical calibration period. After bias correction, we statistically downscale the CMIP5 projections using a constructed analog approach similar to the method introduced by Pierce et al. (2014). For a specific CMIP5 model and future day, we find the single best matching historical analog using the entire Red River spatial domain. The final downscaled projections for the future day are the local high-resolution APHRODITE observations that correspond to the historical coarse analog modified by a scaling factor that accounts for differences between the analog and future day (Pierce et al., 2014). For a more detailed description of the bias correction and downscaling methods, please see section S3 of the supporting information.

For the hydrologic modeling, we build a statistical hydrologic model that runs on a monthly time step, since all hydrologic multipliers are applied on a monthly time step in the scenario discovery experiment. A summary of the hydrologic model and its performance over the historical record is provided in section S4 of the supporting information. The monthly model has a Nash-Suttcliffe efficiency of 0.921 in calibration (1961–1990) and 0.940 in validation (1991–2000). To ensure that flood risk is not underestimated, errors are added back to the estimated future streamflows based on the historical error model structure. The results of our scenario evaluation over the downscaled climate projections are presented in section 4.3.

4. Results and Discussion

4.1. Robustness of Trade-off Solutions

The Pareto-approximate set of Red River operating policies discovered from the optimization described in section 3.2 is shown in Figure 6 on a parallel axis plot. In this figure, each line represents a different operating policy that crosses each vertical axis at the objective value it achieves in the base SOW, with the favorable direction along each axis being down. The color of the line represents the percent of generated SOWs in which the policy is able to simultaneously meet each of the performance satisficing thresholds: $J_{\text{Flood}} \leq 2.15$ m, $J_{\text{Hydro}} \geq 25$ GWh/day, and $J_{\text{Max Def}} \leq 350$ m^3/s. Light yellow corresponds to high robustness, while dark purple corresponds to low robustness. While the policies were optimized to minimize the daily squared deficit, the value of the maximum deficit is shown on the far right axis since satisficing thresholds were based on that metric. Satisficing thresholds were set assuming that the Vietnamese government would like to provide protection to the 100-year flood but would be willing to tolerate a reduction of up to 5 GWh/day in hydropower production from the worst performing solution in the base SOW and a 10% increase in the maximum deficit of the worst performing solution in the base SOW. More lenient thresholds were set for the hydropower and deficit objectives since Vietnam is heavily investing in additional sources of electric power (Asian Development Bank, 2016), and more efficient agricultural practices could reduce the impacts of severe deficits. To visualize the performance of the optimized solutions on each of these thresholds individually, see section S1 of the supporting information.

Across the solutions in the Pareto approximate set, all three of these performance goals can only be met simultaneously in about 10–30% of generated SOWs. While this may sound low, the generated worlds are not equally likely. In fact, some may be extremely unlikely. As such, this metric should not be interpreted as a reliability but as a measure for comparing the relative robustness of alternative solutions. Looking first at the most robust solutions with respect to flooding and the deficit, highlighted in Figure 6, one can see that they are near optimal on those objectives in the base SOW. However, the most robust solution for hydropower production is suboptimal in the base SOW. The reason for this is because the satisficing threshold of 25 GWh/day in the worst first percentile year is below the 30–50 GWh/day range in which the near-optimal hydropower solutions are most robust (see Figure S1 in the supporting information). To achieve satisfactory performance across all objectives, the most robust solution, shaded yellow, heavily favors flood protection and deficit minimization

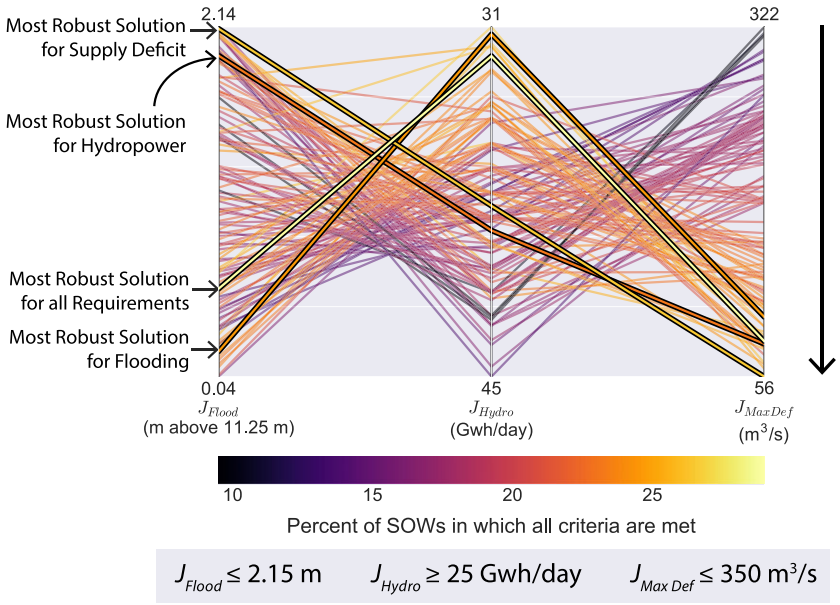

Figure 6. Parallel axis plot of the trade-off set in the base state of the world (SOW), with each solution shaded by its robustness across all system objectives. Each line represents a different operating policy, crossing the three axes at the objective value it achieves on the corresponding objective in the base SOW. The shading for robustness corresponds to the percent of generated SOWs in which each solution meets all of the minimum performance criteria for the three objectives. The most robust solutions for flooding and the deficit are near optimal on those objectives in the base SOW, while the most robust solution for hydropower production is suboptimal in the base SOW. The most robust solution across all objectives favors flood protection and deficit minimization, with strong sacrifices in hydropower performance.

over hydropower production in the base SOW. In section 4.2 we investigate which combinations of deeply uncertain factors cause each of these four highlighted solutions to fail to meet the minimum performance criteria for each objective.

4.2. Scenario Discovery

As stated in section 3.4, we further analyze how the deeply uncertain hydrologic and socioeconomic factors influence the performance of alternative Red River operating policies using logistic regression. Figure 7 illustrates this analysis for the most robust solution with respect to flooding to show where even this policy is unable to meet the flooding performance criterion. According to the logistic regression model, the most important factors in determining whether or not this solution can succeed on the flooding objective are the multipliers on the log-space mean flow, m_μ, the log-space standard deviation, m_σ, and the log-space amplitude of the first harmonic, m_{C_1} (see Tables S1 and S2 of the supporting information for more details).

Figures 7a and 7d show where the most robust solution for flooding is able to provide protection to the 100-year flood as a function of these three factors. These panels represent two-dimensional projections of the 1,000 SOWs generated in our scenario discovery experiment, with each circle representing a different SOW. The circles are shaded light blue if the policy was able to meet the flooding criterion in that world and dark red if it was not. The *x* axis in both panels is the log-space mean multiplier, while the *y* axis in panel a is the log-space amplitude of the first harmonic multiplier and the *y* axis in panel b is the log-space standard deviation multiplier.

Not surprisingly, wetter worlds ($m_\mu > 1$) increase the probability of failure. However, if the wetter worlds are accompanied by decreases in the log-space amplitude of the first harmonic ($m_{C_1} < 1$) or the annual standard deviation ($m_\sigma < 1$), the most robust flood solution can tolerate greater increases in the log-space mean flow. This is because a decrease in the amplitude of the first harmonic results in drier monsoons and wetter dry seasons. Since flooding is only of concern during the monsoon season, an increase in the mean annual flow can be tolerated if the within-year flow distribution becomes more even, reducing flow peaks during the monsoon. Similarly, a decrease in the annual standard deviation results in less extreme annual highs and lows, so an increase in the mean flow can be tolerated if interannual variability decreases.

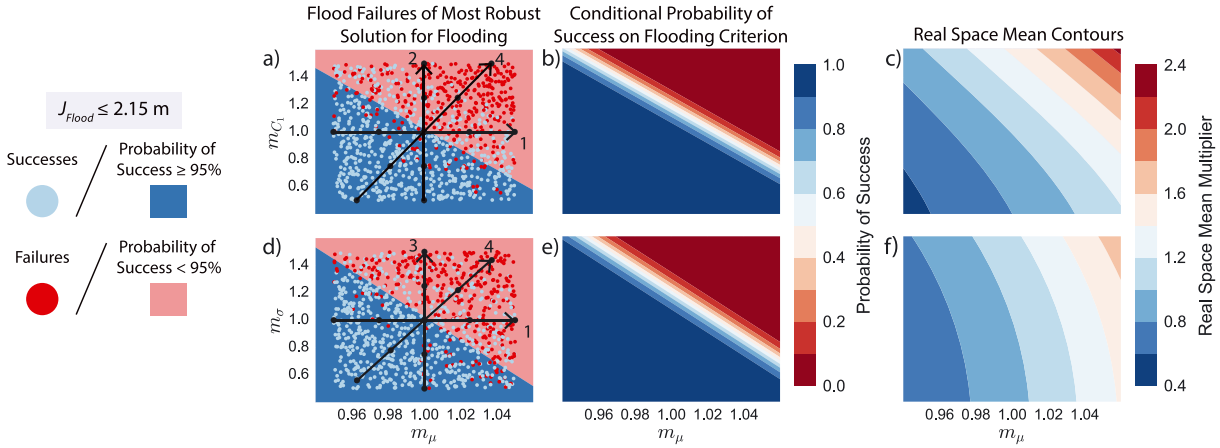

Figure 7. Successes and failures of the most robust solution for flooding (panels a and d). The log-space mean multiplier, m_μ, amplitude of the first harmonic multiplier, m_{C_1}, and standard deviation multiplier, m_σ are the most important factors controlling performance. The probability of failure as a function of each of these factors as predicted by the logistic regression is shown in panels b and e. These probability contours differ greatly from the real-space mean contours shown in panels c and f.

Not only does the logistic regression model quantify which factors are most important in explaining the ability of this solution to provide protection to the 100-year flood but it also estimates the probability of success as a function of these factors. These probabilities are shown in Figures 7b and 7e as a function of the variables on each axis, with the third factor held constant at its base value. Given that the three most important factors of the log-space mean, log-space standard deviation, and log-space amplitude of the first harmonic all change the real-space mean, an interesting question is whether these failure contours simply correspond to constant values of the real-space mean. Figures 7c and 7f show that this is not the case, as the real-space mean contours do not run parallel to the probability contours of the logistic regression and are in fact nonlinear. More importantly, comparing the contours of the logistic regression with the real-space mean contours, it can be seen that when the log-space mean (*x* axis in all figures) decreases, failures due to increases in the log-space amplitude of the monsoonal cycle (*y* axis in panel b), and even more so, the log-space standard deviation (*y* axis in panel e) occur sooner than would be expected if the real-space mean were the only predictor of failure. This highlights the importance of stress testing reservoir operations over worlds with greater intraannual and interannual variability to capture failure mechanisms that would not be discovered by only exploring the impacts of the mean changing uniformly in time. Preparing for these failures could be critical for monsoonal systems since climate models consistently project wetter monsoons but do not agree on the sign of change for dry season precipitation (Ray et al., 2015).

In addition to illustrating the importance of exploring the impacts of a wide range of plausible hydrologic changes beyond the mean, the logistic regression can also be used to define success and failure regions. Since the effects of overtopping the dikes surrounding Hanoi could be catastrophic for the city, we assume a conservative classifier of success and failure regions in which the success region is defined by having at least a 95% chance of providing protection to the 100-year flood within that SOW. The success region is shaded dark blue under the dots in Figures 7a and 7d, while the failure region is shaded light red. With this classifier, it can be seen that any increase in one of the three factors from their base value of 1 results in movement to the failure region, indicating high sensitivity of even the most robust solution for flooding to each of these hydrologic factors. This strong sensitivity of flood protection to one's estimate of simple streamflow statistics underscores the potential dangers of optimizing to stationary hydrology (Milly et al., 2008).

To visualize how flood events change as conditions deviate from this safe operating space, we have plotted time series of flows during the year of the 100-year flood when operating with the most robust solution for flooding in different SOWs. These events are shown in Figures 8a–8d. Each of the events illustrated in panels a–d corresponds to a different point along the SOW trajectories shown in Figures 7a and 7d. The dark blue events illustrate the dynamics resulting from operating in the most favorable SOW along each trajectory, while the dark red events illustrate the dynamics resulting from operating in the least favorable SOW, with a gradient of colors representing the SOWs in between. The events in Figure 8a correspond to the points along SOW Trajectory 1, drawn in Figures 7a and 7d, in which only the log-space mean multiplier, m_μ, is varied

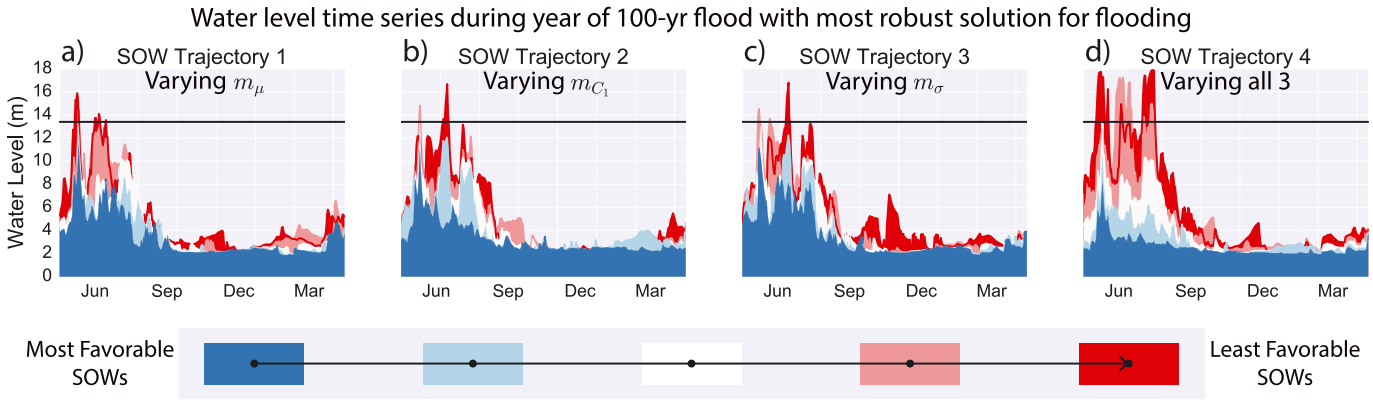

Figure 8. Illustration of how the mechanism of flood failures changes as a function of the log-space mean, log-space standard deviation, and log-space amplitude of the first harmonic. Panel a shows the effect of moving along the points in Trajectory 1 of Figures 7a and 7d (varying m_μ), panel b shows the same for Trajectory 2 of Figure 7a (varying m_{C_1}), panel c for Trajectory 3 of Figure 7d (varying m_σ), and panel d for Trajectory 4 in Figures 7a and 7d (varying all three perpendicular to the classifying boundary). Blue events correspond to the most favorable worlds along the trajectory, while red events represent the least favorable, with a gradient for the worlds sampled in between. The black lines in panels a–d represent the minimum performance thresholds for the maximum water level at Hanoi in the worst first percentile year. SOW = state of the world.

while all other factors are held constant at their base values. Figure 8b shows how events change along SOW Trajectory 2, drawn in Figure 7a, in which only the log-space amplitude of the first harmonic, m_{C_1}, is varied. Figure 8c illustrates the same for SOW Trajectory 3, drawn in Figure 7d, in which only the log-space annual standard deviation, m_σ, is varied. Finally, Figure 8d shows how events change along SOW Trajectory 4, drawn in both Figures 7a and 7d, in which all three of these hydrologic factors vary together perpendicular to the classifying boundary.

The first notable observation from Figures 8a–8d is that the log-space mean, log-space standard deviation, and log-space amplitude of the monsoonal cycle all influence the real-space mean but change flood events in different ways. Looking first at the influence of the log-space mean on flood events shown in panel a, when the most robust solution for flooding operates in the base SOW shown in white, it just barely provides protection to the 100-year event. As the mean decreases/increases (blue/red events), the water levels decrease/increase at all times of the year, with greater differences observed during the monsoon season since the mean multiplier is applied in log-space. This year-round increase in the flows results in near-overtopping routinely occurring in really wet worlds. When only the log-space amplitude of the first harmonic is varied (panel b), there is little difference in flows outside of the monsoon season and changes during the monsoon season apply mostly to the peaks. As a result, increasingly flashy flows cause overtopping or near overtopping when only the amplitude of the first harmonic increases. Floods therefore become more severe but of shorter duration. The effect of the log-space annual standard deviation (panel c) lies somewhere in between: While severe flood events are generated, those causing near overtopping are not as flashy as those caused solely by increases in the log-space amplitude of the first harmonic nor as persistent as those caused by increases in the log-space mean. Considering all of these changes together (panel d), it can be seen how the effects of these factors compound each other to result in severe flood events of long duration. These different failure mechanisms elucidate the need to explore the effects of a broad range of changing streamflow characteristics for effective flood risk assessment.

Moving to Figure 9 the same analysis is applied to analyze the performance of the most robust solutions for hydropower and the deficit. Looking first at panels a and b in the first row (and Tables S3 and S4 of the supporting information), it can be seen that hydropower performance failures for this solution were also found to be most influenced by the log-space annual mean multiplier, m_μ (x axis in panels a and b), log-space multiplier on the amplitude of the first harmonic, m_{C_1} (y axis in panel a), and log-space annual standard deviation multiplier, m_σ (y axis in panel b). To classify successes and failures on the hydropower threshold, we choose the 50% probability contour from the logistic regression model. Since alternative energy sources can be substituted for hydropower, stakeholders will likely be less concerned about always being able to satisfy this performance measure. With this classification, the hydropower success region for the most robust solution for hydropower encompasses nearly all SOWs. Once again, this failure boundary is far from parallel

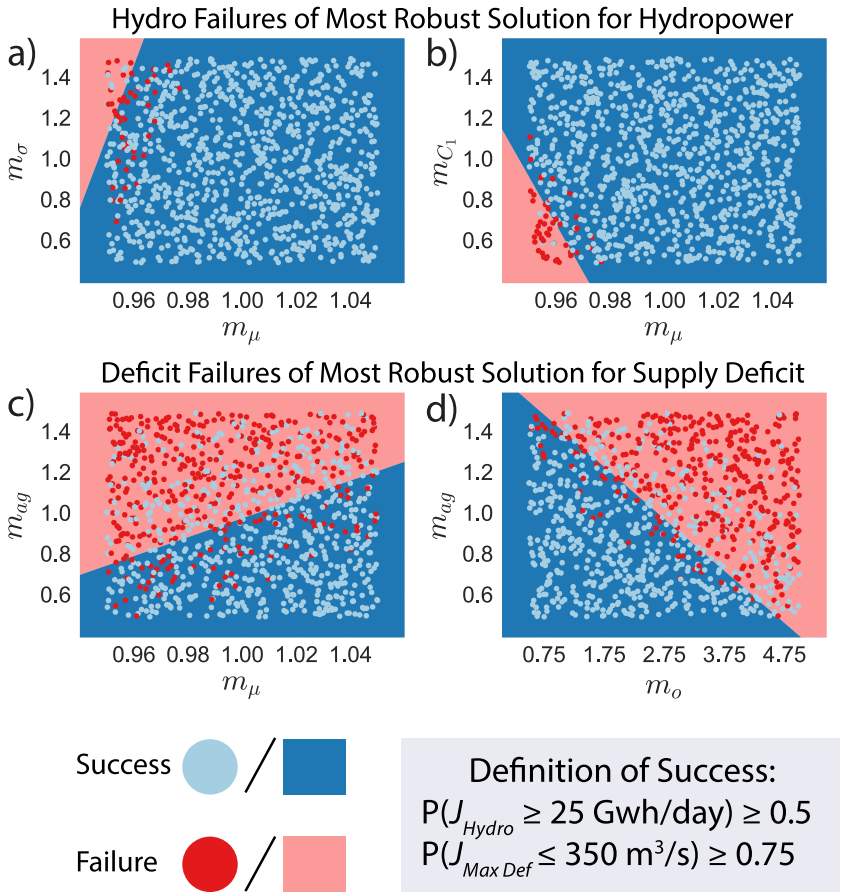

Figure 9. Successes and failures of the most robust solution for hydropower (panels a and b) and the most robust solution for the deficit (panels c and d). The most important factors controlling performance on the hydropower threshold are the log-space mean multiplier, m_μ, amplitude of the first harmonic multiplier, m_{C_1}, and standard deviation multiplier, m_σ. The most important factors controlling performance on the deficit threshold are the log-space mean multiplier, m_μ, agricultural demand multiplier, m_{ag}, and other demand multiplier, m_o.

to the real-space mean contours, illustrating the important effects of changing interannual variability and seasonality on hydropower production in addition to flood protection.

Not only is this policy's ability to provide satisfactory hydropower production less sensitive to the deeply uncertain factors than the ability of the most robust solution for flooding to provide flood protection, but its success and failure regions are opposite of those for flooding. For hydropower production, wetter worlds ($m_\mu > 1$) increase production, especially if accompanied by an increase in the amplitude of the annual cycle ($m_{C_1} > 1$), resulting in greater production during the monsoon (panel a). While the amplitude of the annual cycle impacts both hydropower production and flooding, its effect on hydropower is weaker than for flooding because an increased amplitude will also result in drier dry seasons. Consequently, energy production during the dry season will decrease in these worlds, negating some of the monsoonal benefits.

The interaction between the log-space mean annual flow and its standard deviation is also weaker for hydropower performance than for flooding, as shown in panel b. This is because m_σ has a weaker influence on hydropower production than m_μ. The interaction between m_μ and m_σ is also of opposite sign for hydropower than for flooding. Increased standard deviations result in higher annual highs and lower annual lows, but since the hydropower objective specifically targets the worst first percentile, the lower lows result in more failures. Consequently, an increase in the standard deviation of annual flow is bad for both hydropower production and flooding, whereas an increase in the mean or amplitude of the first harmonic is bad for flooding but good for hydropower production.

For the deficit objective, Figures 9c and 9d (and Tables S5 and S6 of the supporting information) show that a different suite of deeply uncertain factors emerge as most important in determining when the most robust solution for the deficit fails to meet the deficit satisficing threshold. The log-space mean flow is still important, but instead of interacting primarily with the amplitude of the first harmonic and annual standard deviation, it interacts more with the multipliers on agricultural demand, m_{ag} (y axis in panels a and b), and other demands such as industrial and municipal, m_o (x axis in panel b). In fact, the greatest interaction is between the agricultural and other demand growth multipliers (panel b). These findings further highlight the need to explore the effects of a wide range of factors in bottom-up risk assessments, as socioeconomic factors may be as or more important than climatic factors.

For the deficit objective, we define failure boundaries using the 75% probability contour from the logistic regression model. Since 70% of the Vietnamese population is employed in agriculture (Nguyen et al., 2002), performing well on the deficit is important for the region's food security, but the consequences of failing to provide sufficient water supply are not as severe as the consequences of flooding Hanoi. The 75% cut-off is therefore chosen to model a moderately risk-averse stakeholder who values confidence in performance on the deficit more than for hydropower but less than for flooding. Panel a shows that, with this classifier, any decrease in the log-space mean or increase in agricultural demand cannot be tolerated, as even in the base SOW, the deficit threshold can only be met with 72% reliability, meaning the base SOW lies outside the safe operating space. Moving to panel b, one can see that greater increases in other demands can be tolerated, as the failure boundary lies at a multiplier value of 2.75 on this factor when there is no growth in agricultural demand. Some policies from the multiobjective optimization were discovered that satisfied the deficit threshold with >75% reliability in the base SOW, but in fewer sampled worlds, illustrating a trade-off between optimality and robustness. These findings suggest that designing satisfactory operations for water supply needs both now and in the future is challenging, necessitating the implementation of more efficient agricultural practices and multisectoral demand management strategies.

4.3. Scenario Evaluation

Figures 7 and 9 provide insight into which deeply uncertain factors increase the probability that a control policy is able to meet individual performance objectives in different SOWs and why. Decision makers evaluating operating policies for the multireservoir Red River system should closely track each of these factors as additional observations become available to determine if they should reoptimize the reservoir operating policies, incentivize demand management strategies, or perhaps build new infrastructure or import additional power or food. Given the proximity of the base hydrologic factors to the flooding boundary, they may even want to reoptimize policies now across a range of plausible deeply uncertain SOWs to improve robustness on the flooding objective. Operators in the Red River basin, and Southeast Asia generally, should be particularly concerned by this proximity to failure since the multireservoir operations analyzed here were optimized assuming perfect coordination. Knowing the plausibility of failure under such idealized operations will help engineers designing operations for existing and planned dams to prioritize (i) which system objectives and corresponding performance thresholds they should be most concerned about improving, and (ii) to which critical hydrologic factors they should be robust.

To guide operators in this redesign process, we track how these streamflow multipliers change in downscaled climate projections to identify which combinations of hydrologic changes may be more likely to occur than others and whether or not those combinations fall outside a given policy's success region. Here we define a success region using the most robust solution across all requirements (see Figure 6). We again determine failure boundaries for this solution using logistic regression (see Tables S7 and S8 of the supporting information), with success probabilities of at least 95% and 50% used to define the success region on the flooding and hydropower satisficing criteria, respectively. By combining thresholds for both of these objectives, the resulting success region is narrower than those illustrated in Figures 7 and 9. Because the deficit is controlled primarily by socioeconomic factors and the climate projections can only be used as proxies for hydrologic changes, we do not consider failures on the deficit in defining the success region for this analysis.

The spread of traces across the CMIP5 models is illustrated in Figure 10 on top of the success and failure regions of the most robust solution across all requirements. Each CMIP5 model is represented by a different shape and is colored according to the RCP under which the projection was run. Many model/color combinations repeat because an ensemble of initial conditions were run. Three snapshots of these traces are shown: 1980–2009 (panels a and d), 2025–2054 (panels b and e), and 2070–2099 (panels c and f). The first row of Figure 10 shows

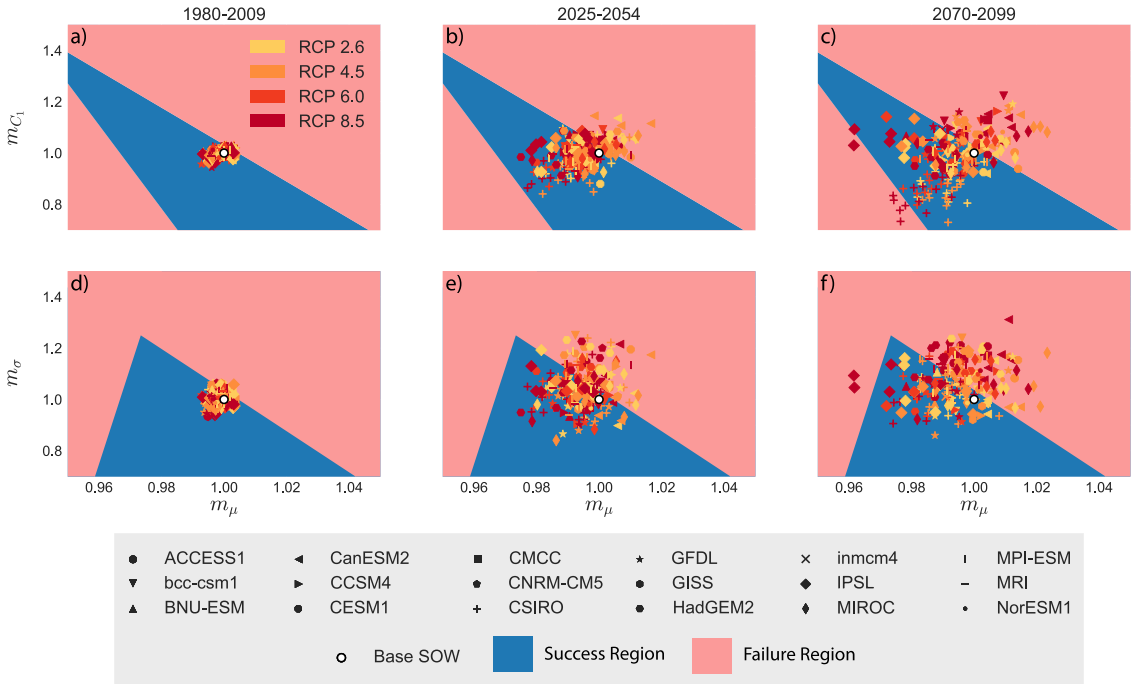

Figure 10. Snapshots of hydrologic factors tracked through CMIP5 model projections laid atop the success and failure regions of the most robust solution across all requirements shown in Figure 6. CMIP5 model labels refer to the institution; see the Acronyms section for the full model names. With respect to the log-space annual mean, m_μ, and log-space amplitude of the first harmonic, m_{C_1} (panels a–c), the projections quickly depart from the base state of the world. Of particular concern are the many projections that move to the right of the success region, resulting in failure to provide protection to the 100-year flood. With respect to the log-space annual mean and standard deviation, m_σ, (panels d–f), most of the general circulation model (GCM) projections experience increased interannual variability, migrating to the flooding failure region by the end of the century.

combinations of the multiplier on the log-space annual mean flow, m_μ, on the *x* axis and the multiplier on the log-space amplitude of the first harmonic, m_{C_1}, on the *y* axis. The second row does the same but with the multiplier on the log-space annual standard deviation, m_σ, on the *y* axis.

While the first time stamp is only 4 years after the defined climatology from 1976 to 2005, at which each multiplier is set to 1, the model projections already begin to migrate from the base SOW to the boundary of the success region. This likely would not be of concern since the synthetic streamflows in this study were based on a larger climatology of 1960–2010. However, marching forward in time, the spread in model projections significantly increases, with many models migrating well outside the success region. In particular, the projections tend to move along Trajectory 4 from Figures 7a and 7d, where flooding events become severe and of long duration (see Figure 8d). If only changes in the real-space mean were explored, the severity of future floods induced by these changes would be underestimated. Knowing this, dam operators in the region should prioritize coordination of operating policies for existing and planned reservoirs to provide flood protection to more severe flood events than historical observations suggest they should expect.

Another concerning feature of these projections is that, while there is no general tendency across models for m_μ or m_{C_1} to increase or decrease, m_σ increases more frequently than it decreases. This is consistent with the theory that global warming will increase climate variability (Trenberth, 2011). Given that increased variability results in poorer performance on both flooding and hydropower production in the tails (see Figures 7 and 9), operators may want to consider reoptimizing policies to more variable worlds.

One final concern about the model projections is that they appear to cluster more by institution than by RCP. This is likely due to the fact that streamflow is more directly influenced by precipitation than temperature, and the response of monsoonal precipitation to the different RCP forcings is more nuanced and uncertain than the response of temperature to forcing (Knutti & Sedláček, 2013). Sabeerali et al. (2015) also observe that precipitation projections for the South Asian monsoon tend to cluster more by model than by RCP. While clustering of projections from models within the same family is a well-understood phenomenon (Knutti et al., 2013; Masson & Knutti, 2011; Steinschneider, McCrary, Mearns et al., 2015), we believe this behavior has only been

analyzed for projections run with a common forcing scenario. Future research should formally test whether and why precipitation projections tend to cluster more by model or RCP, both globally and regionally. The clustering observed here, and the fact that past studies have found greater variability in projections across models than across forcing scenarios (Déqué et al., 2007), highlight that top-down climate risk assessments should consider multiple models, not just multiple forcing scenarios, to prevent severe underestimation of future climate uncertainty.

5. Conclusions and Future Work

This study advances scenario discovery analyses for multireservoir systems, contributing a new method for jointly exploring the effects of changing monsoonal dynamics and socioeconomic demands on river basin management. We demonstrate this method on the Red River basin in Vietnam to evaluate how multisectoral trade-offs in the basin are impacted by different plausible futures. While we find the system to be fairly robust with respect to hydropower production, several hydrologic and socioeconomic factors threaten the system's ability to protect Hanoi from severe flooding and to provide sufficient water supply for agriculture. Specifically, we find the log-space mean annual flow, annual standard deviation, and amplitude of the annual monsoonal cycle critically impact flood risks to Hanoi. We also find that agricultural and other demand growth could result in severe deficits during the dry season. The influence of all of these factors illustrates the utility of our method in better capturing possible future risks to multireservoir systems serving multiple conflicting demands.

In particular, combining the influences of all of these factors on multisectoral trade-offs in the basin, we find that reservoir operating policies optimized to stationary conditions can only satisfy performance requirements across the three sectors within a corridor of hydrologic conditions. Furthermore, many downscaled climate projections evolve to SOWs far from this region, especially to regions threatened by flooding. Fortunately, knowing which hydrologic factors drive system performance enables the design of more robust and adaptive policies. For example, the most important factors can be used as signposts of change, with factor combinations near the boundaries of the success region serving as triggers for reoperations. Alternatively, the state dependence of the operating policies can be exploited to design more adaptive operations by explicitly incorporating information on the most important factors, automatically updating operations as planners observe climatic changes that refine their estimates of these factors through time.

While the discovery of which hydrologic and socioeconomic factors most influencing system performance could guide water managers in designing more robust operations for the Red River basin and other monsoonal systems, there are many additional uncertain factors beyond the hydrologic and socioeconomic factors sampled here that could further influence operational success. For example, sedimentation of dams could reduce hydropower production and degrade the downstream ecology (Kummu & Varis, 2007; Kummu et al., 2010; Vörösmarty et al., 2003; Wild & Loucks, 2014), as could sand mining now prevalent in the delta. Sea level rise will almost certainly increase flood risk, while also degrading the quality of freshwater resources in the irrigation canals through salinization. Furthermore, the log-space rescaling of stationary synthetic flows used to generate alternative hydrologic worlds in this study does not enable an analysis of event-scale changes in flows, such as increased daily variability. While the analysis performed here is an informative first cut examination of how operations should adapt to better meet conflicting demands in the Red River basin, future work should explore the impacts of these additional uncertainties in order to further improve bottom-up risk assessments, and ultimately, water resources system robustness.

Acronyms

ACCESS	Australian Community Climate and Earth System Simulator (versions 1.1 and 1.3)
ANN	artificial neural network
BCC-CSM	Beijing Climate Center Climate System Model (version 1.1)
BNU-ESM	Beijing Normal University Earth System Model
CanESM2	The second generation Canadian Earth System Model
CCSM4	NCAR Community Climate System Model 4
CESM1	NCAR Community Earth System Model 1 (Biogeochemistry and Community Atmosphere Model 5)
CMCC	Centro Euro-Mediterraneo per I Cambiamenti Climatici (Carbon Earth System Model and Climate Model with a resolved Stratrosphere)

CMIP	Coupled Model Intercomparison Project
CNRM-CM5	Centre National de Recherches Météorologiques Coupled global climate Model, version 5
CSIRO	Commonwealth Scientific and Industrial Research Organisation (Mark 3.6.0 and Mark 3L version 1.2)
DAPP	Dynamic Adaptive Policy Pathways
EDCDFm	equidistant cumulative distribution function matching
EMODPS	Evolutionary Multiobjective Direct Policy Search
ENSO	El Nino Southern Oscillations
FDC	flow duration curve
GCM	general circulation model
GFDL	NOAA Geophysical Fluid Dynamics Laboratory (Coupled Model version 3, the isopycnal Earth system model using the Generalized Ocean Layer Dynamics code base, and the pressure-based vertical coordinates Earth system model using the Modular Ocean Model version 4.1 code base)
GISS	NASA Goddard Institute for Space Studies (ModelE version 2 HYCOM ocean model and Russell ocean model)
HadGEM2	Hadley Global Environment Model 2 (Atmosphere-Ocean, Carbon Cycle and Earth System models)
HB	Hoa Binh reservoir
HN	Hanoi
IMRR	Integrated and sustainable water Management of Red Thai Binh Rivers system in changing climate
INM-CM4	Russian Institute for Numerical Mathematics Climate Model 4
ITCZ	Intertropical Convergence Zone
IPSL	Institut Pierre Simon Laplace
MIROC	Model for Interdisciplinary Research on Climate (version 5, Earth System Model and atmospheric chemistry coupled Earth System Model)
MORDM	Many Objective Robust Decision Making
MOEA	multiobjective evolutionary algorithm
MPI-ESM	Max Planck Institut für Meteorologie Earth System Model (low and medium resolution versions)
MRI	Meteorological Research Institute (atmosphere-ocean Coupled General Circulation model 3 and Earth System Model version 1)
NorESM1	Norwegian Earth System Model version 1 (medium resolution)
RDM	Robust Decision Making
RBF	radial basis function
SL	Son La reservoir
SOW	state of the world
SST	sea surface temperature
TB	Thac Ba reservoir
TQ	Tuyen Quang reservoir

Notation

A	number of RBFs in RBF policies
ag	agricultural demand
aq	aquaculture demand
B	number of inputs to RBF policies
b	radii of RBF policies
C	amplitude of log-space annual and semi-annual cycles describing hydrograph
c	centers of RBF policies
D	daily water supply deficit
d	delta shift of deeply uncertain parameters
e	evaporation
g	value of objective function on daily time step
J	objective function value across all ensemble members
K	number of outputs of RBF policies

M vector of time-varying multipliers on streamflow statistics
m multiplier on deeply uncertain parameters
N number of ensemble members
o other demand
p phase of sin(·) and cos(·) functions
q flow
r reservoir release
s reservoir storage
T number of years per ensemble member
t time
u policy-prescribed release
w weights of RBF policies
x vector of inputs to RBF policies
z water level
η hydropower production per reservoir
μ log-space mean flow
θ vector of RBF parameters w, c, and b
Υ water volume in the canals
Φ operator for the aggregation of g over time
ϕ phase of annual and semiannual cycles describing hydrograph
Ψ statistic used to filter noise of objective function across ensemble members
σ log-space annual flow standard deviation

Acknowledgments
The authors would like to thank Jery Stedinger, Todd Walter, and three anonymous reviewers for helpful suggestions and comments on an earlier draft of this manuscript. This study was partially supported by the National Science Foundation (NSF) through the Network for Sustainable Climate Risk Management (SCRiM) under NSF cooperative agreement GEO-1240507 and the Penn State Center for Climate Risk Management. Any opinions, findings, and conclusions or recommendations expressed in this material are those of the authors and do not necessarily reflect the views of the funding entities. We also acknowledge the World Climate Programme's Working Group on Coupled Modelling, which is responsible for CMIP, and we thank the climate modeling groups (listed in Table S10 of the supporting information) for producing and making available their model output. For CMIP, the U.S. Department of Energy's Program for Climate Model Diagnosis and Intercomparison provides coordinating support and led development of software infrastructure in partnership with the Global Organization for Earth System Science Portals. Code and detailed step-by-step algorithm documentation of the climate downscaling can be found at https://github.com/scrim-network/red_river. All other data used in this study are from the Ministry of Agriculture and Rural Development (MARD) of Vietnam and were collected during the IMRR project (http://xake.elet.polimi.it/imrr/). Because the code for the model, Figures 3–5, 7c and 7f, and S2–S4 contains governmental information on hydropower plants, demand, and streamflow in the basin that is protected by a nondisclosure agreement with the Vietnamese government, it cannot be made public. The code for all other figures can be found at https://github.com/julianneq/RedRiver_MonsoonalDynamics, and the code for the synthetic streamflow generator can be found at https://github.com/julianneq/Kirsch-Nowak_Streamflow_Generator using data for the Susquehanna River basin instead of the Red River basin as an example. Please contact the authors to obtain other data or model results.

References

Anandhi, A., Frei, A., Pierson, D. C., Schneiderman, E. M., Zion, M. S., Lounsbury, D., & Matonse, A. H. (2011). Examination of change factor methodologies for climate change impact assessment. *Water Resources Research*, *47*, W03501. https://doi.org/10.1029/2010WR009104

Asian Development Bank (2016). Vietnam: Energy sector assessment, strategy and road map (Tech. Rep.). Asian Development Bank.

Bankes, S. (1993). Exploratory modeling for policy analysis. *Operations Research*, *41*(3), 435–449.

Bouwer, H. (2000). Integrated water management: Emerging issues and challenges. *Agricultural Water Management*, *45*(3), 217–228.

Brown, C., Ghile, Y., Laverty, M., & Li, K. (2012). Decision scaling: Linking bottom-up vulnerability analysis with climate projections in the water sector. *Water Resources Research*, *48*, W09537. https://doi.org/10.1029/2011WR011212

Cai, W., Borlace, S., Lengaigne, M., Van Rensch, P., Collins, M., Vecchi, G., et al. (2014). Increasing frequency of extreme El Niño events due to greenhouse warming. *Nature Climate Change*, *4*(2), 111–116.

Déqué, M., Rowell, D., Lüthi, D., Giorgi, F., Christensen, J., Rockel, B., et al. (2007). An intercomparison of regional climate simulations for Europe: Assessing uncertainties in model projections. *Climatic Change*, *81*(1), 53–70.

Dessai, S., Hulme, M., Lempert, R., & Pielke, R. Jr (2009). Climate prediction: A limit to adaptation, *Adapting to climate change: Thresholds, values, governance* (pp. 64–78): Cambridge University Press.

Diaz-Nieto, J., & Wilby, R. L. (2005). A comparison of statistical downscaling and climate change factor methods: Impacts on low flows in the River Thames, United Kingdom. *Climatic Change*, *69*(2–3), 245–268.

Dinh, N. Q. (2015). Multi-objective evolutionary algorithm, dynamic and non-dynamic emulators in the design of optimal policies for water resources management (PhD thesis), Politecnico di Milano.

Dittrich, R., Wreford, A., & Moran, D. (2016). A survey of decision-making approaches for climate change adaptation: Are robust methods the way forward? *Ecological Economics*, *122*, 79–89.

Galelli, S., & Castelletti, A. (2013). Tree-based iterative input variable selection for hydrological modeling. *Water Resources Research*, *49*, 4295–4310. https://doi.org/10.1002/wrcr.20339

Galelli, S., Humphrey, G. B., Maier, H. R., Castelletti, A., Dandy, G. C., & Gibbs, M. S. (2014). An evaluation framework for input variable selection algorithms for environmental data-driven models. *Environmental Modelling & Software*, *62*, 33–51. https://doi.org/10.1016/j.envsoft.2014.08.015

Giuliani, M., Castelletti, A., Pianosi, F., Mason, E., & Reed, P. M. (2016). Curses, tradeoffs, and scalable management: Advancing evolutionary multiobjective direct policy search to improve water reservoir operations. *Journal of Water Resources Planning and Management*, *142*, 4015050.

Giuliani, M., Quinn, J. D., Herman, J. D., Castelletti, A., & Reed, P. M. (2017). Scalable multiobjective control for large-scale water resources systems under uncertainty, IEEE Transactions on Control Systems Technology.

Groves, D., Bloom, E., Lempert, R., Fischbach, J., Nevills, J., & Goshi, B. (2014). Developing key indicators for adaptive water planning. *Journal of Water Resources Planning and Management*, *141*, 5014008. https://doi.org/10.1061/(ASCE)WR.1943-5452.0000471

Guo, H., Xu, M., & Hu, Q. (2011). Changes in near-surface wind speed in China: 1969–2005. *International Journal of Climatology*, *31*(3), 349–358.

Haasnoot, M., Kwakkel, J. H., Walker, W. E., & ter Maat, J. (2013). Dynamic adaptive policy pathways: A method for crafting robust decisions for a deeply uncertain world. *Global Environmental Change*, *23*(2), 485–498. https://doi.org/10.1016/j.gloenvcha.2012.12.006

Hadka, D., & Reed, P. (2013). Borg: An auto-adaptive many-objective evolutionary computing framework. *Evolutionary computation*, *21*(2), 231–259.

Hadka, D., & Reed, P. (2015). Large-scale parallelization of the borg multiobjective evolutionary algorithm to enhance the management of complex environmental systems. *Environmental Modelling & Software*, *69*, 353–369.

Hansson, K., & Ekenberg, L. (2002). Flood mitigation strategies for the Red River delta. In *Proceeding of the 2002 Joint CSCE/EWRI of ASCE International Conference on Environmental Engineering, An International Perspective on Environmental Engineering* (pp. 21–24). Niagara Falls, Ont., Canada.

Hao, Z., & Singh, V. P. (2016). Review of dependence modeling in hydrology and water resources. *Progress in Physical Geography*, *40*(4), 549–578.

Hartmann, D., Klein Tank, A., Rusticucci, M., Alexander, L., Brönnimann, S., Charabi, Y., et al. (2013). Observations: Atmosphere and surface, *Climate change 2013 the physical science basis: Working Group I Contribution to the Fifth Assessment Report of the Intergovernmental Panel on Climate Change* (Vol. 9781107057999, pp. 159–254). Cambridge, United Kingdom and New York, NY: Cambridge University Press.

Herman, J. D., & Giuliani, M. (2018). Policy tree optimization for threshold-based water resources management over multiple timescales. *Environmental Modelling & Software*, *99*, 39–51.

Herman, J. D., Reed, P. M., Zeff, H. B., & Characklis, G. W. (2015). How should robustness be defined for water systems planning under change? *Journal of Water Resources Planning and Management*, *141*(10), 4015012.

Herman, J. D., Zeff, H. B., Lamontagne, J. R., Reed, P. M., & Characklis, G. W. (2016). Synthetic drought scenario generation to support bottom-up water supply vulnerability assessments. *Journal of Water Resources Planning and Management*, *142*(11), 4016050.

Herman, J. D., Zeff, H. B., Reed, P. M., & Characklis, G. W. (2014). Beyond optimality: Multistakeholder robustness tradeoffs for regional water portfolio planning under deep uncertainty. *Water Resources Research*, *50*, 7692–7713. https://doi.org/10.1002/2014WR015338

Hermans, L. M., Haasnoot, M., ter Maat, J., & Kwakkel, J. H. (2017). Designing monitoring arrangements for collaborative learning about adaptation pathways. *Environmental Science & Policy*, *69*, 29–38.

Hijioka, Y., Lin, E., Pereira, J. J., Corlett, R., Cui, X., Insarov, G., et al. (2014). Chapter 24: Asia, Working Group II contribution to the IPCC Fifth Assessment Report Climate Change.

Hsu, P.-c., Li, T., & Wang, B. (2011). Trends in global monsoon area and precipitation over the past 30 years. *Geophysical Research Letters*, *38*, L08701. https://doi.org/10.1029/2011GL046893

Huijun, W. (2002). The instability of the East Asian summer monsoon-ENSO relations. *Advances in Atmospheric Sciences*, *19*(1), 1–11.

Jiang, Y., Luo, Y., Zhao, Z., & Tao, S. (2010). Changes in wind speed over China during 1956–2004. *Theoretical and Applied Climatology*, *99*(3-4), 421–430.

Jiang, D.-B., Wang, H.-J., Drange, H., & Lang, X.-M. (2004). Instability of the East Asian summer monsoon-ENSO relationship in a coupled global Atmosphere-Ocean GCM. *Chinese Journal of Geophysics*, *47*(6), 1098–1103.

Juneng, L., & Tangang, F. T. (2005). Evolution of ENSO-related rainfall anomalies in Southeast Asia region and its relationship with atmosphere-ocean variations in Indo-Pacific sector. *Climate Dynamics*, *25*(4), 337–350.

Kane, R. (1999). El niño timings and rainfall extremes in India, Southeast Asia and China. *International Journal of Climatology: A Journal of the Royal Meteorological Society*, *19*(6), 653–672.

Kasprzyk, J. R., Nataraj, S., Reed, P. M., & Lempert, R. J. (2013). Many objective robust decision making for complex environmental systems undergoing change. *Environmental Modelling and Software*, *42*, 55–71. https://doi.org/10.1016/j.envsoft.2012.12.007

Katz, R. W., & Brown, B. G. (1992). Extreme events in a changing climate: Variability is more important than averages. *Climatic Change*, *21*(3), 289–302.

Kirsch, B. R., Characklis, G. W., & Zeff, H. B. (2013). Evaluating the impact of alternative hydro-climate scenarios on transfer agreements: A practical improvement for generating synthetic streamflows. *Journal of Water Resources Planning and Management*, *139*(4), 396–406. https://doi.org/10.1061/(ASCE)WR.1943-5452.0000287

Knight, F. H. (1921). *Risk, uncertainty, and profit*. Boston, MA: Houghton Mifflin.

Knutti, R., Masson, D., & Gettelman, A. (2013). Climate model genealogy: Generation CMIP5 and how we got there. *Geophysical Research Letters*, *40*, 1194–1199. https://doi.org/10.1002/grl.50256

Knutti, R., & Sedláček, J. (2013). Robustness and uncertainties in the new CMIP5 climate model projections. *Nature Climate Change*, *3*(4), 369–373. https://doi.org/10.1038/nclimate1716

Kroll, C. N., Croteau, K. E., & Vogel, R. M. (2015). Hypothesis tests for hydrologic alteration. *Journal of Hydrology*, *530*, 117–126.

Kummu, M., Lu, X., Wang, J., & Varis, O. (2010). Basin-wide sediment trapping efficiency of emerging reservoirs along the Mekong. *Geomorphology*, *119*(3), 181–197.

Kummu, M., & Varis, O. (2007). Sediment-related impacts due to upstream reservoir trapping, the lower Mekong river. *Geomorphology*, *85*(3), 275–293.

Kwadijk, J. C. J., Haasnoot, M., Mulder, J. P. M., Hoogvliet, M. M. C., Jeuken, A. B. M., van der Krogt, R. A. A., et al. (2010). Using adaptation tipping points to prepare for climate change and sea level rise: A case study in the Netherlands. *Wiley Interdisciplinary Reviews: Climate Change*, *1*(5), 729–740. https://doi.org/10.1002/wcc.64

Le Ngo, L., Madsen, H., Rosbjerg, D., & Pedersen, C. B. (2008). Implementation and comparison of reservoir operation strategies for the Hoa Binh reservoir, Vietnam using the MIKE 11 model. *Water Resources Management*, *22*(4), 457–472.

Lempert, R., Popper, S., & Bankes, S. (2002). Confronting surprise. *Social Science Computer Review*, *20*(4), 420–440.

Lempert, R. J., Popper, S. W., & Bankes, S. C. (2003). *Shaping the next one hundred years: New methods for quantitative, long-term policy analysis RAND*. Santa Monica: CA.

Li, H., Sheffield, J., & Wood, E. F. (2010). Bias correction of monthly precipitation and temperature fields from intergovernmental panel on climate change AR4 models using equidistant quantile matching. *Journal of Geophysical Research*, *115*, D10101. https://doi.org/10.1029/2009JD012882

Mach, K., & Mastrandrea, M. (2014). *Climate change 2014: Impacts, adaptation, and vulnerability*. In C. B. Field & V. R. Barros (Eds.) (Vol. 1). Cambridge and New York: Cambridge University Press.

Maier, H. R., Guillaume, J. H., van Delden, H., Riddell, G. A., Haasnoot, M., & Kwakkel, J. H. (2016). An uncertain future, deep uncertainty, scenarios, robustness and adaptation: How do they fit together? *Environmental Modelling & Software*, *81*, 154–164.

Masson, D., & Knutti, R. (2011). Climate model genealogy. *Geophysical Research Letters*, *38*, L08703. https://doi.org/10.1029/2011GL046864

Milly, P. C. D., Betancourt, J., Falkenmark, M., Hirsch, R. M., Kundzewicz, Z. W., Lettenmaier, D. P., & Stouffer, R. J. (2008). Climate change: Stationarity is dead: Whither water management? *Science*, *319*(5863), 573–574. https://doi.org/10.1126/science.1151915

Nazemi, A., Wheater, H. S., Chun, K. P., & Elshorbagy, A. (2013). A stochastic reconstruction framework for analysis of water resource system vulnerability to climate-induced changes in river flow regime. *Water Resources Research*, *49*, 291–305. https://doi.org/10.1029/2012WR012755

Nguyen, T. C., Do, N. H., Nguyen, T., & Egashira, K. (2002). Agricultural development in the Red River delta, Vietnam: Water management, land use, and rice production.

Nowak, K., Prairie, J., Rajagopalan, B., & Lall, U. (2010). A nonparametric stochastic approach for multisite disaggregation of annual to daily streamflow. *Water Resources Research*, *46*, W08529. https://doi.org/10.1029/2009WR008530

Pierce, D. W., Cayan, D. R., Maurer, E. P., Abatzoglou, J. T., & Hegewisch, K. C. (2015). Improved bias correction techniques for hydrological simulations of climate change. *Journal of Hydrometeorology*, *16*(6), 2421–2442.
Pierce, D. W., Cayan, D. R., & Thrasher, B. L. (2014). Statistical downscaling using localized constructed analogs (LOCA). *Journal of Hydrometeorology*, *15*(6), 2558–2585.
Poff, N. L., Brown, C. M., Grantham, T. E., Matthews, J. H., Palmer, M. A., Spence, C. M., et al. (2015). Sustainable water management under future uncertainty with eco-engineering decision scaling. *Nature Climate Change*, *6*, 25–34.
Poff, N. L., & Zimmerman, J. K. (2010). Ecological responses to altered flow regimes: A literature review to inform the science and management of environmental flows. *Freshwater Biology*, *55*(1), 194–205.
Pruyt, E., & Islam, T. (2016). On generating and exploring the behavior space of complex models. *System Dynamics Review*, *31*, 220–249.
Quinn, J., Reed, P., Giuliani, M., & Castelletti, A. (2017). Rival framings: A framework for discovering how problem formulation uncertainties shape risk management trade-offs in water resources systems. *Water Resources Research*, *53*, 7208–7233. https://doi.org/10.1002/2017WR020524
Räsänen, T. A., & Kummu, M. (2013). Spatiotemporal influences of ENSO on precipitation and flood pulse in the Mekong River basin. *Journal of Hydrology*, *476*, 154–168.
Ray, P. A., Bonzanigo, L., Wi, S., Yang, Y.-C. E., Karki, P., García, L. E., et al. (2018). Multidimensional stress test for hydropower investments facing climate, geophysical and financial uncertainty. *Global Environmental Change*, *48*, 168–181.
Ray, P. A., Yang, Y.-C. E., Wi, S., Khalil, A., Chatikavanij, V., & Brown, C. (2015). Room for improvement: Hydroclimatic challenges to poverty-reducing development of the Brahmaputra River basin. *Environmental Science & Policy*, *54*, 64–80.
Richter, B. D., Baumgartner, J. V., Powell, J., & Braun, D. P. (1996). A method for assessing hydrologic alteration within ecosystems. *Conservation Biology*, *10*(4), 1163–1174.
Rossi, S. (2016). A vulnerability analysis of the Red River basin, Vietnam under co-varying climate and socio-economic changes (Master's thesis), Politecnico di Milano.
Sabeerali, C., Rao, S. A., Dhakate, A., Salunke, K., & Goswami, B. (2015). Why ensemble mean projection of South Asian monsoon rainfall by CMIP5 models is not reliable? *Climate Dynamics*, *45*(1-2), 161–174.
Salas, J. D., Delleur, J. W., Yevjevich, V., & Lane, W. L. (1980). *Applied Modeling of Hydrologic Time Series*. Littleton, CO: Water Resources Publication.
Shen, S., & Lau, K.-M. (1995). Biennial oscillation associated with the East Asian summer monsoon and tropical sea surface temperatures. *Journal of the Meteorological Society of Japan. Series II*, *73*(1), 105–124.
Singhrattna, N., Rajagopalan, B., Kumar, K. K., & Clark, M. (2005). Interannual and interdecadal variability of Thailand summer monsoon season. *Journal of Climate*, *18*(11), 1697–1708.
Starr, C. (1969). Social benefit versus technological risk. *Science*, *165*(3899), 1232–1238.
Steinschneider, S., McCrary, R., Mearns, L. O., & Brown, C. (2015). The effects of climate model similarity on probabilistic climate projections and the implications for local, risk-based adaptation planning. *Geophysical Research Letters*, *42*, 5014–5044. https://doi.org/10.1002/2015GL064529
Steinschneider, S., McCrary, R., Wi, S., Mulligan, K., Mearns, L. O., & Brown, C. (2015). Expanded decision-scaling framework to select robust long-term water-system plans under hydroclimatic uncertainties. *Journal of Water Resources Planning and Management*, *141*(11), 4015023.
Timmermann, A., Oberhuber, J., Bacher, A., Esch, M., Latif, M., & Roeckner, E. (1999). Increased El Niño frequency in a climate model forced by future greenhouse warming. *Nature*, *398*(6729), 694–697.
Trenberth, K. E. (2011). Changes in precipitation with climate change. *Climate Research*, *47*(1–2), 123–138.
Vautard, R., Cattiaux, J., Yiou, P., Thépaut, J.-N., & Ciais, P. (2010). Northern Hemisphere atmospheric stilling partly attributed to an increase in surface roughness. *Nature Geoscience*, *3*(11), 756–761.
Vogel, R. M., Sieber, J., Archfield, S. A., Smith, M. P., Apse, C. D., & Huber-Lee, A. (2007). Relations among storage, yield, and instream flow. *Water Resources Research*, *43*, W05403. https://doi.org/10.1029/2006WR005226
Vörösmarty, C. J., Green, P., Salisbury, J., & Lammers, R. B. (2000). Global water resources: Fulnerability from climate change and population growth. *Science*, *289*(5477), 284–288.
Vörösmarty, C. J., Meybeck, M., Fekete, B., Sharma, K., Green, P., & Syvitski, J. P. (2003). Anthropogenic sediment retention: Major global impact from registered river impoundments. *Global and Planetary Change*, *39*(1), 169–190.
Wang, Y.-J., Cheng, H., Edwards, R. L., An, Z., Wu, J., Shen, C.-C., & Dorale, J. A. (2001). A high-resolution absolute-dated late Pleistocene monsoon record from Hulu Cave, China. *Science*, *294*(5550), 2345–2348.
Wang, B., Liu, J., Kim, H.-J., Webster, P. J., & Yim, S.-Y. (2012). Recent change of the global monsoon precipitation (1979–2008). *Climate Dynamics*, *39*(5), 1123–1135.
Wang, L., Sarnthein, M., Erlenkeuser, H., Grimalt, J., Grootes, P., Heilig, S., et al. (1999). East Asian monsoon climate during the late Pleistocene: High-resolution sediment records from the South China Sea. *Marine Geology*, *156*(1), 245–284.
Whateley, S., Steinschneider, S., & Brown, C. (2014). A climate change range-based method for estimating robustness for water resources supply. *Water Resources Research*, *50*, 8944–8961. https://doi.org/10.1002/2014WR015956
Wild, T. B., & Loucks, D. P. (2014). Managing flow, sediment, and hydropower regimes in the Sre Pok, Se San, and Se Kong rivers of the Mekong basin. *Water Resources Research*, *50*, 5141–5157. https://doi.org/10.1002/2014WR015457
Xu, Z., Takeuchi, K., & Ishidaira, H. (2004). Correlation between El Niño–Southern Oscillation (ENSO) and precipitation in South-east Asia and the Pacific region. *Hydrological Processes*, *18*(1), 107–123.
Yancheva, G., Nowaczyk, N. R., Mingram, J., Dulski, P., Schettler, G., Negendank, J. F., et al. (2007). Influence of the Intertropical Convergence Zone on the East Asian monsoon. *Nature*, *445*(7123), 74–77.
Yang, Y. E., Wi, S., Ray, P. A., Brown, C. M., & Khalil, A. F. (2016). The future nexus of the Brahmaputra River basin: climate, water, energy and food trajectories. *Global Environmental Change*, *37*, 16–30.
Yatagai, A., Kamiguchi, K., Arakawa, O., Hamada, A., Yasutomi, N., & Kitoh, A. (2012). APHRODITE: Constructing a long-term daily gridded precipitation dataset for Asia based on a dense network of rain gauges. *Bulletin of the American Meteorological Society*, *93*(9), 1401–1415.
Yu, B., Zhu, T., Breisinger, C., & Hai, N. M. (2010). Impacts of climate change on agriculture and policy options for adaptation, International Food Policy Research Institute (IFPRI).
Zatarain Salazar, J., Reed, P. M., Quinn, J. D., Giuliani, M., & Castelletti, A. (2017). Balancing exploration, uncertainty and computational demands in many objective reservoir optimization. *Advances in Water Resources*, *109*, 196–210.
Zhou, T., Gong, D., Li, J., & Li, B. (2009). Detecting and understanding the multi-decadal variability of the East Asian summer monsoon–recent progress and state of affairs. *Meteorologische Zeitschrift*, *18*(4), 455–467.